

Reduced late endosome/lysosome function promotes SLE through chronic PI3K activity and SHP-1/SHIP-1 defects

SunAh Kang,¹ Andrew J. Monteith,¹ Liubov Arbeeveva,² Karissa Grier,³ Shruti Saxena Beem,² Anthony C. Trujillo,² Xinyun Bi,¹ Kai Sun,³ Rebecca E. Sadun,³ Mithu Maheswaranathan,³ Megan E.B. Clowse,³ Saira Z. Sheikh,² Jennifer L. Rogers,³ and Barbara J. Vilen¹

¹Department of Microbiology and Immunology and ²Division of Rheumatology, Allergy, and Immunology, Thurston Arthritis Research Center, University of North Carolina, Chapel Hill, North Carolina, USA. ³Division of Rheumatology and Immunology, Duke University Medical Center, Durham, North Carolina, USA.

Degradation of cellular waste from phagocytosis, endocytosis, and autophagy occurs through hydrolases that become activated during acidification of late endosomes and lysosomes (LELs). In our cross-sectional study, we showed diminished LEL acidification and the accumulation of surface-bound nucleosome on monocytes, dendritic cells, B cells, neutrophils, and T cells from patients with systemic lupus erythematosus (SLE). Diminished acidification and exocytosis of undegraded IgG-immune complexes were evident in active, but not inactive, disease. This was supported by our murine study in which LEL acidification was diminished, promoting exocytosis and the accumulation of cell surface IgG-immune complexes. Mechanistically, LEL dysfunction was induced by chronic PI3K activation in lupus-prone MRL/lpr mice. We also showed that on a non-autoimmune C57BL/6 background, deficiency in SHP-1 and inhibition of SHIP-1 activity were sufficient to recapitulate LEL dysfunction found in MRL/lpr mice. Non-acidic LELs were evident in the majority of patients and associated with SLEDAI arthritis, rash, and nephritis. The high frequency of LEL dysfunction in SLE suggests that it could serve as a biomarker identifying a specific disease endotype.

Introduction

Systemic lupus erythematosus (SLE) is a multi-organ autoimmune disease with underlying genetic, epigenetic, and environmental components. Genome-wide association studies identified more than 80 confirmed risk loci (1), suggesting widespread allelic heterogeneity. Loci include genes related to lymphocyte activation, clearance of immune complexes (ICs), nucleic acid sensing, and interferon (IFN) signaling (2). Although recent therapeutic advances, including targeted biologics, have enhanced treatment options in SLE, strategies to limit the frequency and severity of active disease (3) remain challenging because factors triggering active disease remain undefined.

IgG-immune complexes (IgG-ICs) form when IgG autoantibodies bind cell-derived self-antigens, including those exposed on apoptotic blebs. IgG-ICs are associated with heightened type I IFN responses via Fcγ receptor (FcγR) activation on plasmacytoid dendritic cells, and they correlate with enhanced disease activity and lupus nephritis (4). Early studies showed that bone marrow cells from SLE patients contained undegraded, intracellular apoptotic material (5), and these were termed “lupus erythematosus cells.” However, whether the undegraded material was due to abnormal late endosome/lysosome (LEL) function was not investigated. Later, studies of murine and human SLE identified several possible mechanisms that might increase IgG-ICs. These included heightened cell death (6), diminished phagocytosis (7), and defects in opsonins that tag apoptotic debris for removal (8).

LELs maintain cellular homeostasis by degrading macromolecules entering cells by endocytosis, phagocytosis, and autophagy (9). The luminal pH of endosomes/lysosomes is maintained between 4.5 and 6.5 (compared with cytoplasmic pH of ~7.0) because of the activity of an ATP-dependent proton pump present in LEL membranes (10). Acidification of LELs facilitates release of ligands from internalized receptors and activates hydrolytic enzymes that degrade cargo (11). When the pH of LELs increases, degradation is reduced, and LELs migrate from the perinuclear region of the cell to the plasma membrane

Conflict of interest: BJV reports a pending patent application, “Composition and Methods for Crosslinking Fc Receptors,” and incorporation of Autoimmune Therapeutic, Inc.

Copyright: © 2026, Kang et al. This is an open access article published under the terms of the Creative Commons Attribution 4.0 International License.

Submitted: January 28, 2025

Accepted: February 4, 2026

Published: February 10, 2026

Reference information: *JCI Insight*. 2026;11(6):e191767.
<https://doi.org/10.1172/jci.insight.191767>.

(12), where they fuse and release their contents extracellularly, a process termed exocytosis (9). Similarly, when LEL degradation is diminished, cargo in the LELs that is bound by transmembrane-spanning receptors is inserted into the plasma membrane (9).

We identified that diminished LEL acidification is evident in murine SLE (13–15), reducing the degradation of inflammatory IgG-ICs, and promoting the accumulation of nuclear self-antigen on the surface of dendritic cells (DCs), macrophages (Mφs), B cells, and T cells (13). Delayed degradation of IgG-ICs in endosomes prolongs activation of Toll-like receptors (TLRs) and disrupts the integrity of the phagolysosomal membrane, allowing IgG-ICs to leak into the cytosol (15). This provides ligands for innate cytosolic sensors including AIM2 and TRIM21, leading to pyroptosis, heightened IRF7, and increased IFN- α production. Mechanistically, mTORC2 diminishes maturation and acidification of LELs in Mφs via chronic activation of Fc γ R signaling (14). A role for Fc γ Rs in murine SLE is also supported by bone marrow chimeric studies showing that expression of activating Fc γ Rs (Fc γ RI, Fc γ RIII, Fc γ RIV) on hematopoietic cells, rather than kidney mesangial cells, is required for lupus nephritis (16). Further, loss of Fc γ RI on myeloid cells from MRL/*lpr* mice is sufficient to attenuate B cell expansion, BAFF secretion, autoantibody production, and lupus nephritis (13). Thus, cellular homeostasis is disrupted in murine lupus when IgG-ICs and chronic Fc γ R signaling diminish LEL acidification.

In this study, we find that LEL dysfunction is evident in multiple splenic hematopoietic cell types in mice, multiple genetically unrelated models of SLE, and blood cells of patients with SLE. We show that diminished LEL acidification associates with active, but not inactive, disease. Undegraded LEL cargo accumulates on the surface of monocytes (Mo), DCs, neutrophils, and T and B cells, with the highest levels on B cells. Non-acidic LELs are evident in 67% of patients with SLE, indicating a high frequency in the SLE population. Further, non-acidic LELs are found in 92% of patients with active lupus nephritis, 63% with Systemic Lupus Erythematosus Disease Activity Index (SLEDAI) arthritis, and 73% with SLEDAI rash. Mechanistically, LEL dysfunction in mice is induced by PI3K activation, in part coupled to Fc γ RI. Deletion and/or inactivation of SHP-1 and SHIP-1 in C57BL/6 mice is sufficient to recapitulate LEL dysfunction in MRL/*lpr* mice. Our discovery of an acidification defect in LELs during active SLE is important because it could be a biomarker identifying a specific lupus endotype, and/or serve as the basis for a therapeutic aimed at maintaining disease inactivity. It is noteworthy that defects in lysosome function are emerging in multiple inflammatory diseases, including neurodegenerative diseases such as Parkinson's and Alzheimer's (17), metabolic dysfunction-associated steatotic liver disease (18), and lysosomal storage diseases (19). Although the molecular events underlying lysosomal defects in these diseases are unique, our studies add murine and human lupus to this growing list of inflammatory diseases with inefficient removal of waste.

Results

Multiple hematopoietic cell types exhibit LEL dysfunction. Previous studies showed that bone marrow-derived Mφs (BMMφs) from MRL/*lpr* mice exhibit diminished LEL acidification (15). In all cell types, peak acidification occurred at 30 minutes, with deacidification beginning at 60 minutes (15). To assess whether impaired acidification was evident in other cell types, we compared the LEL hydrogen ion concentration ($[H^+]$) in splenic hematopoietic cells from MRL/*lpr* and C57BL/6 (B6) mice of different ages following stimulation with IgG-ICs. $[H^+]$ is an inversely related linear readout of pH. In 9- to 10-week-old mice, the LEL $[H^+]$ in CD11b⁺ myeloid cells was comparable in B6 and MRL/*lpr* mice (Figure 1A); however, as disease progressed, the $[H^+]$ was decreased 12.6-fold in 15- to 16-week-old MRL/*lpr* mice (Figure 1, A–C; see Supplemental Table 1 for fold change and pH values; supplemental material available online with this article; <https://doi.org/10.1172/jci.insight.191767DS1>). B cells (Figure 1B) and DCs (Figure 1C) from MRL/*lpr* mice also showed decreased $[H^+]$ as disease progressed (B cells: 2.3-fold, 15–18 weeks; DCs: 3-fold, >18 weeks). In comparison with B6 mice, the $[H^+]$ was also decreased in LELs of MRL/*lpr* neutrophils (2.1-fold) and T cells (3.2-fold) at 15–16 weeks (Supplemental Figure 1, A and B).

To corroborate that decreased $[H^+]$ (\uparrow pH) in LELs was biologically relevant, we quantified hydrolase activity in hematopoietic cells. The hydrolase activity in B6 CD11b⁺ myeloid cells (Figure 1D, 9–10 weeks) was comparable to that in cells from MRL/*lpr* mice; however, MRL/*lpr* B cells (Figure 1E) and DCs (Figure 1F) had lower hydrolase activity compared with B6 cells (9–10 weeks). Concomitant with declining $[H^+]$, hydrolase activity in CD11b⁺ myeloid cells and B cells from MRL/*lpr* mice was reduced 2.6- to 6.6-fold as mice aged (12 to >18 weeks), consistent with the idea that reduced $[H^+]$ (\uparrow pH) elicits functional consequences in LELs. Despite numerically reduced hydrolase activity in MRL/*lpr* DCs (3.2- to 4.0-fold; 12

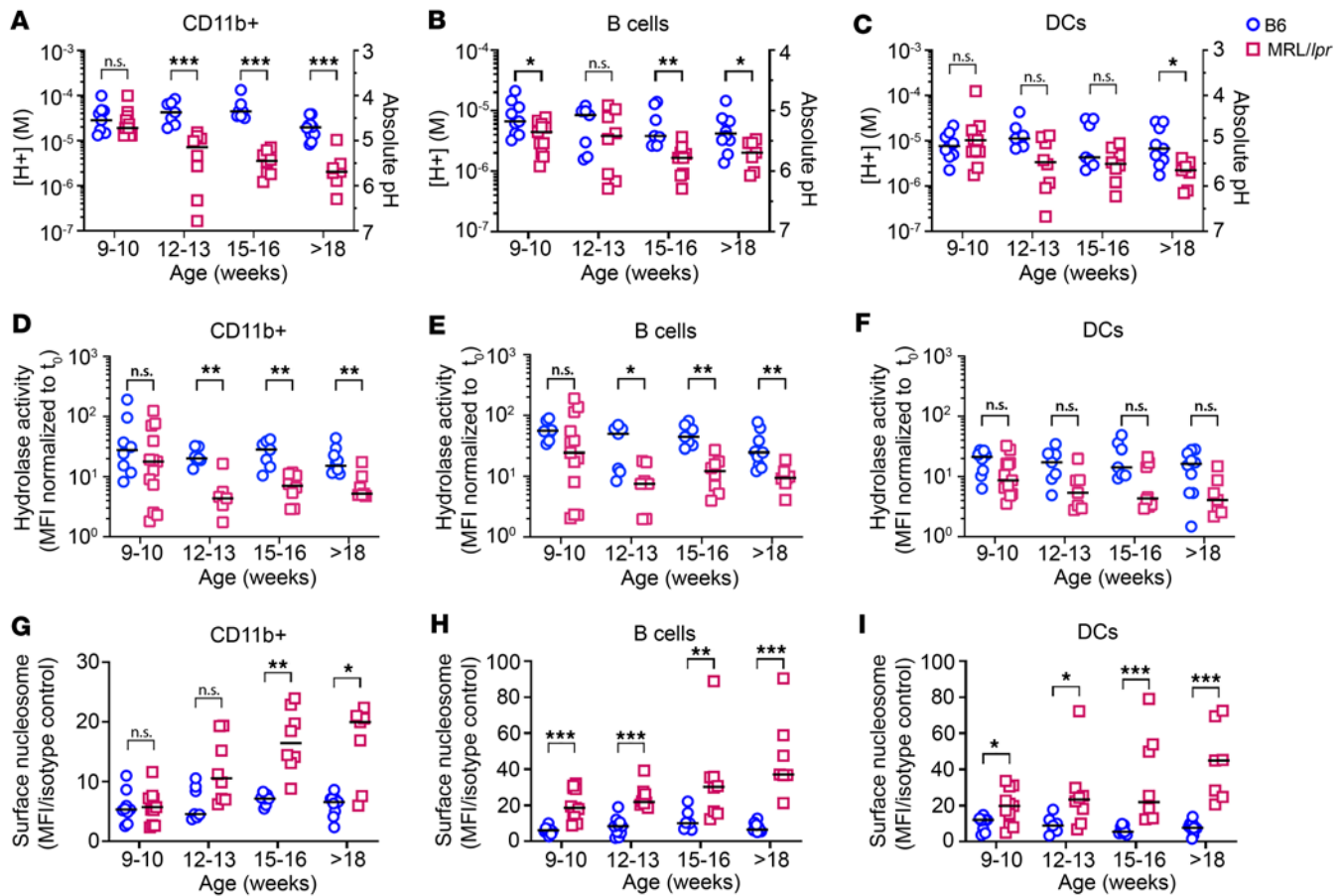


Figure 1. LEL dysfunction is evident in multiple hematopoietic cell types. Splenocytes from C57BL/6 (circles) or MRL/lpr (squares) mice at different ages were stimulated with IgG-ICs (30 μ L IgG-ICs per 0.25×10^6 cells). (A–C) LEL pH was measured by flow cytometry 30 minutes after treatment in CD11b⁺ myeloid cells (CD3⁺CD19⁺CD11b⁺) (A), B cells (CD3⁺CD19⁺) (B), and DCs (CD3⁺CD19⁺CD11b⁺CD11c^{hi}) (C). Absolute pH was calculated using a standard curve, then converted to $[H^+]$ ($pH = -\log_{10}[H^+]$). (D–F) Flow cytometry was used to measure LEL hydrolase activity (D–F), and the levels of surface nucleosomes on splenocytes from mice of different ages (G–I). $N = 7$ –11 mice, 5–8 experiments per age group. Statistical analysis used Mann-Whitney test (A–I). * $P < 0.05$, ** $P < 0.01$, *** $P < 0.001$. Bars indicate median. See Supplemental Table 1 for absolute pH and fold change calculations.

to >18 weeks), the values did not achieve statistical significance (Figure 1F), suggesting that DCs maintain hydrolase activity better than myeloid cells or B cells. This might reflect that as professional antigen-presenting cells, DCs predominantly use cysteine proteases in late endosomes, and their activation occurs at higher pH (5.0–5.5) in comparison with lysosomes of CD11b⁺ myeloid cells (20).

In MRL/lpr mice, diminished acidification reduces the degradation of LEL cargo (13, 15); however, cell homeostasis is maintained through exocytosis (9). To assess whether diminished LEL acidification and hydrolase activity promote exocytosis, we quantified the levels of surface-bound nucleosome, a nuclear self-antigen in IgG-ICs. We found that splenic CD11b⁺ myeloid cells from B6 and MRL/lpr mice (9–10 weeks) did not increase surface nucleosome levels, consistent with their ability to acidify and activate hydrolases; however, as MRL/lpr mice aged beyond 18 weeks, the surface nucleosome levels on CD11b⁺ myeloid cells were 3-fold higher than those in B6 (Figure 1G). B cells and DCs (Figure 1, H and I) from 9- to 10-week-old MRL/lpr mice showed surface nucleosome levels that were 3- and 1.6-fold higher than B6, respectively, suggesting that exocytosis may occur earlier, or that these cells may have lower LEL capacity. As MRL/lpr mice aged beyond 18 weeks, surface nucleosome levels on B cells and DCs were increased further, to 5.8-fold compared with B6. The surface nucleosome levels on T cells and neutrophils (16–17 weeks) from MRL/lpr mice were increased 2.1-fold (compared with B6) (Supplemental Figure 1, C and D). Collectively, data from MRL/lpr mice show reduced LEL function in CD11b⁺ myeloid cells, DCs, B and T cells, and neutrophils, which worsens as mice progress to end-stage disease.

Diminished LEL acidification is evident in genetically unrelated NZM2410 mice. To assess whether LEL dysfunction was evident in other murine lupus models, we compared B6 and MRL/lpr mice with MRL/MpJ, B6.lpr, NZM2410/J (21), and Sle123 (22). After 30 minutes of IgG-IC stimulation, the $[H^+]$ in splenic

CD11b⁺ myeloid cells from MRL/*lpr* mice was decreased 22.2-fold ($P = 0.0035$) in comparison with B6 at 30 minutes (t_{30}); in splenic CD11b⁺ myeloid cells from NZM2410/J, decreased 25.3-fold ($P = 0.0023$); from B6.Sle123, decreased 16.8-fold ($P = 0.0216$); from MRL/MpJ, decreased 12.6-fold ($P = 0.0060$); and from B6.*lpr*, decreased 1.5-fold ($P = 0.5058$) (Figure 2A). LEL acidification in B6 B cells was lower than that in myeloid cells; nonetheless, the [H⁺] in MRL/*lpr* B cells was still decreased 2.2-fold ($P = 0.0271$); in NZM2410, 2.1-fold ($P = 0.0779$); in MRL/MpJ, 1.9-fold ($P = 0.1453$); and B6.*lpr* showed a 1.6-fold increase in [H⁺] ($P = 0.1428$) (Figure 2B).

Exocytosis signifies undegraded cargo in LELs. To measure exocytosis, we preloaded BMMφs with fluorochrome-tagged IgG-ICs, establishing t_0 levels (maximum surface fluorescence). IgG-ICs entered cells through phagocytosis, and after 24 hours of incubation the surface fluorescence was reduced. Fluorescent IgG-ICs that were not degraded returned to the cell surface via exocytosis at 72 hours (t_{72}), resulting in comparable levels of surface fluorescence with t_0 level. B6 BMMφs did not undergo exocytosis, showing decreased surface fluorescence at t_{72} (35-fold decreased, $P = 0.0001$) compared with t_0 . MRL/*lpr* BMMφs at t_{72} showed increased fluorochrome-tagged IgG-ICs on the cell surface compared with t_0 levels (1.7-fold, $P \leq 0.0001$), as did NZM2410 (1.3-fold, $P = 0.28$), MRL/MpJ (1-fold, $P = 0.981$), and B6.Sle123 (1.1-fold, $P = 0.8299$), indicative of exocytosis of undegraded LEL cargo (Figure 2C). These data show that diminished acidification is conferred by the MRL/MpJ background or the SLE123 quantitative trait loci. The findings that diminished acidification and exocytosis are evident in genetically unrelated models of lupus raise the possibility that LEL dysfunction might be evident in human SLE.

Active SLE patients show diminished LEL acidification and hydrolase activity. To address whether LEL dysfunction was evident in human SLE, we cross-sectionally analyzed peripheral blood cells from 57 healthy controls (HCs) and 81 SLE patients. Patients were grouped by disease activity (hybrid SELENA-SLEDAI; henceforth SLEDAI) as inactive (SLEDAI ≤ 5 , $n = 44$), moderately active (SLEDAI 6–11, $n = 24$), or highly active (SLEDAI ≥ 12 , $n = 13$) (23). In our cohort (65% Black, 33% White, 9% Hispanic, 89% female, mean age 40 ± 14 years, mean length of disease 11 ± 9.5 years), all were anti-nuclear antibody positive, 32% had day-of-visit renal involvement, 56% had historic renal disease, and 80% were prescribed hydroxychloroquine (HCQ) (Supplemental Table 2). As in mice, peak acidification of blood hematopoietic cells occurred at 30 minutes, with deacidification beginning at 60 minutes. The [H⁺] and hydrolase activity in Mo from inactive patients were comparable to those in HCs (Figure 3, A and B, Supplemental Table 3, and Supplemental Figure 2). Mo from moderately active patients showed a 4.2-fold reduction in [H⁺] ($P = 0.0002$) and a 2-fold reduction in hydrolase activity ($P = 0.04$), while highly active patients showed a 6.5-fold reduction in [H⁺] ($P = 0.0004$) and a 2.7-fold reduction in hydrolase activity ($P = 0.007$). B cells from inactive patients showed [H⁺] comparable to that of HCs ($P = 0.14$), while hydrolase activity was decreased 2.1-fold ($P = 0.03$) (Figure 3, C and D). B cells from moderately active patients showed a reduction of 3.2-fold in [H⁺] ($P = 0.007$) and of 3.0-fold ($P = 0.008$) in hydrolase activity, and highly active patients showed a reduction of 4.6-fold in [H⁺] ($P = 0.0009$) and of 3.1-fold in hydrolase ($P = 0.04$). LELs in DCs from HCs and inactive SLE patients showed comparable [H⁺] ($P = 0.99$), while hydrolase activity was decreased 2.3-fold ($P = 0.03$) (Figure 3, E and F). Compared with HCs, DCs from moderately active patients showed a 5.8-fold reduction in [H⁺] ($P = 0.002$) with a 2.9-fold decrease in hydrolase activity ($P = 0.01$), and highly active patients an 8.3-fold reduction in [H⁺] ($P = 0.02$) with a 2.4-fold decrease in hydrolase activity ($P = 0.01$). This shows that, as in murine lupus, reduced LEL acidification (\uparrow pH) and hydrolase activity are evident in Mo, DCs, and B cells from SLE patients with moderately or highly active disease, while acidification in inactive disease is comparable to that in HCs. The exception is DCs and B cells from inactive patients, which show modestly reduced hydrolase activity. This might reflect the differences in hydrolases in late endosomes versus lysosomes, or the duration of sustained activity of hydrolases in DCs and B cells, which predominantly degrade cargo in late endosome.

To assess associations between reduced LEL [H⁺] and disease activity, we calculated the proportion of patients with low [H⁺] in each SLEDAI group (SLEDAI ≤ 5 , 6–11, or ≥ 12), then used the Cochran-Armitage test to identify trends between the proportions. The proportion of patients with low [H⁺] increased as the SLEDAI groups increased in disease activity. Patients with “non-acidic” LELs had [H⁺] lower than a cutoff that was set at 1.8-fold above the mean [H⁺] of HCs for each cell type (Mo, $P = 0.001$; B cells, $P = 0.004$; DCs $P = 0.001$) (Figure 3G). These data suggest an association between SLE disease activity and diminished LEL acidification. The proportion of patients whose Mo showed low hydrolase activity also increased across SLEDAI groups ($P = 0.02$; Figure 3H), except in B cells ($P = 0.37$) or DCs ($P = 0.14$), likely

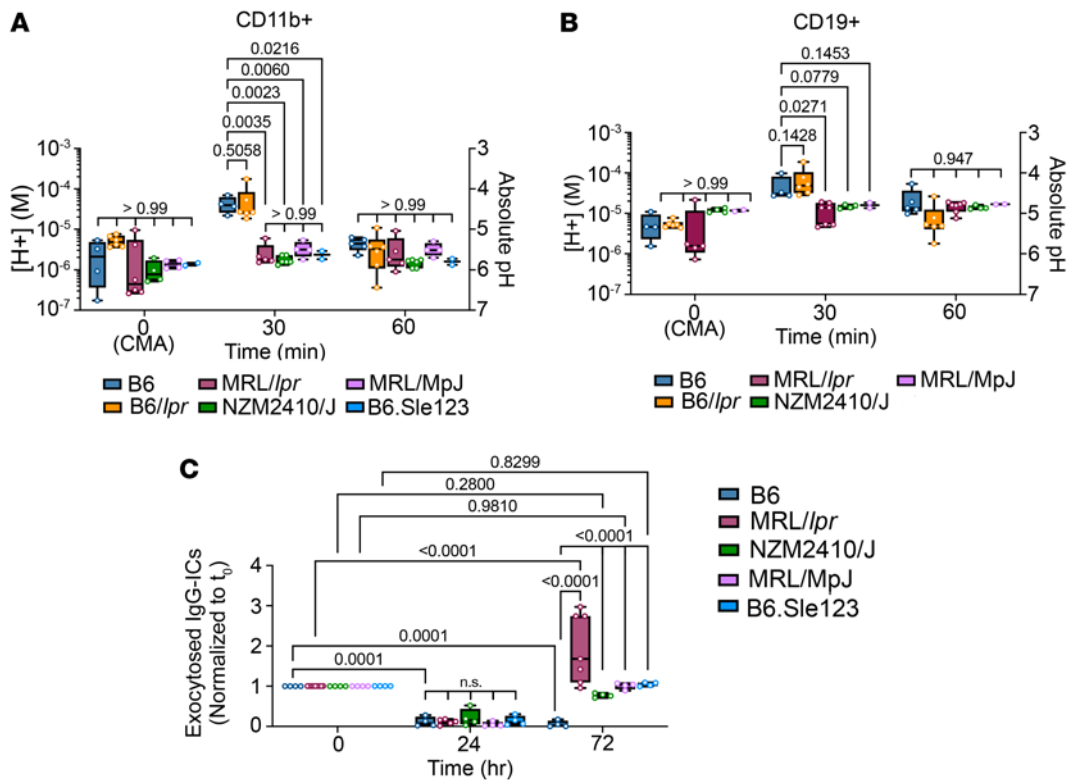


Figure 2. Multiple murine lupus models show diminished [H⁺] and exocytosis of IgG-ICs to the plasma membrane. Splenocytes from the indicated models were stimulated with IgG-ICs (30 μ L IgG-ICs per 0.25×10^6 cells). (A and B) At designated times, LEL pH was measured using flow cytometry in myeloid cells (CD3⁺CD19⁺CD11b⁺) (A) and B cells (CD3⁺CD19⁺) (B). vATPase activity in unstimulated samples [t_0 (CMA)] was inhibited with concanamycin A (CMA; 2 ng/mL). Absolute pH was calculated using a standard curve. (C) BMM ϕ s were preloaded (t_0) with Alexa Fluor 488-labeled IgG-ICs, and exocytosis was measured at designated times. Surface-bound fluorescence was assessed by subtraction of internalized fluorescence (surface quenched) from total (unquenched) and normalized to individual t_0 . Statistical analysis used 2-way ANOVA with multiple comparisons (A–C). Adjusted *P* values with significance are shown. $N \geq 2$ (A and B) and $N \geq 4$ (C) from 2–4 separate experiments. Bars, median; boxes, 25th–75th percentiles; whiskers, minimum and maximum values.

because during inactive disease, B cells and DCs have modestly reduced hydrolase activity (Figure 3, D and F). Patients with “low hydrolase” had levels below a cutoff that was established at 1.7-fold above the mean hydrolase of HCs for each cell type. The proportion of patients with low [H⁺] and low hydrolase increased as the SLEDAI groups increased in disease activity (Mo, $P = 0.001$; B cells, $P = 0.003$; DCs, $P = 0.01$) (Figure 3I). Finally, we estimated the frequency of SLE patients (regardless of disease activity) with diminished LEL acidification. In our cohort of 81 patients, 67% had non-acidic LELs in B cells, 65% in Mo, and 57% in DCs (Supplemental Table 5). These data reveal that LEL dysfunction affects a significant portion of SLE patients and suggest an association between SLEDAI groups and the efficiency of LEL function, especially in Mo.

LEL dysfunction is not associated with HCQ treatment. The mechanism of action of HCQ was initially described as alkalinization of LELs, which reduced antigen presentation (24). However, more recent studies show that HCQ-mediated LEL alkalinization is transient, with normal pH restored within 4 hours (25). We reasoned that if HCQ was responsible for disrupting LEL acidification, then regardless of disease activity, non-acidic LELs would be more prevalent among patients prescribed HCQ, compared with those not prescribed HCQ. The data show that 82% of patients with acidic LELs, and 79% of patients with non-acidic LELs (in Mo), were prescribed HCQ. Similar results were found with B cells (74% acidic, 83% non-acidic) and DCs (83% acidic, 78% non-acidic; Table 1). Further, since non-acidic LELs associated with increased disease activity (Figure 3G), we reasoned that if HCQ caused non-acidic LELs, then the proportion of patients prescribed HCQ should increase as disease activity increased. Instead, the proportion prescribed HCQ was similar across SLEDAI groups (82% inactive, 79% moderately active, 69%–77% highly active; Table 1). This suggests that diminished LEL acidification is not a consequence of HCQ, a finding consistent with LEL dysfunction in untreated MRL/lpr mice (13–15). Alternative explanations for the efficacy of HCQ in treating SLE include its ability to intercalate into nucleic acids (26) and inhibit nucleic acid binding to

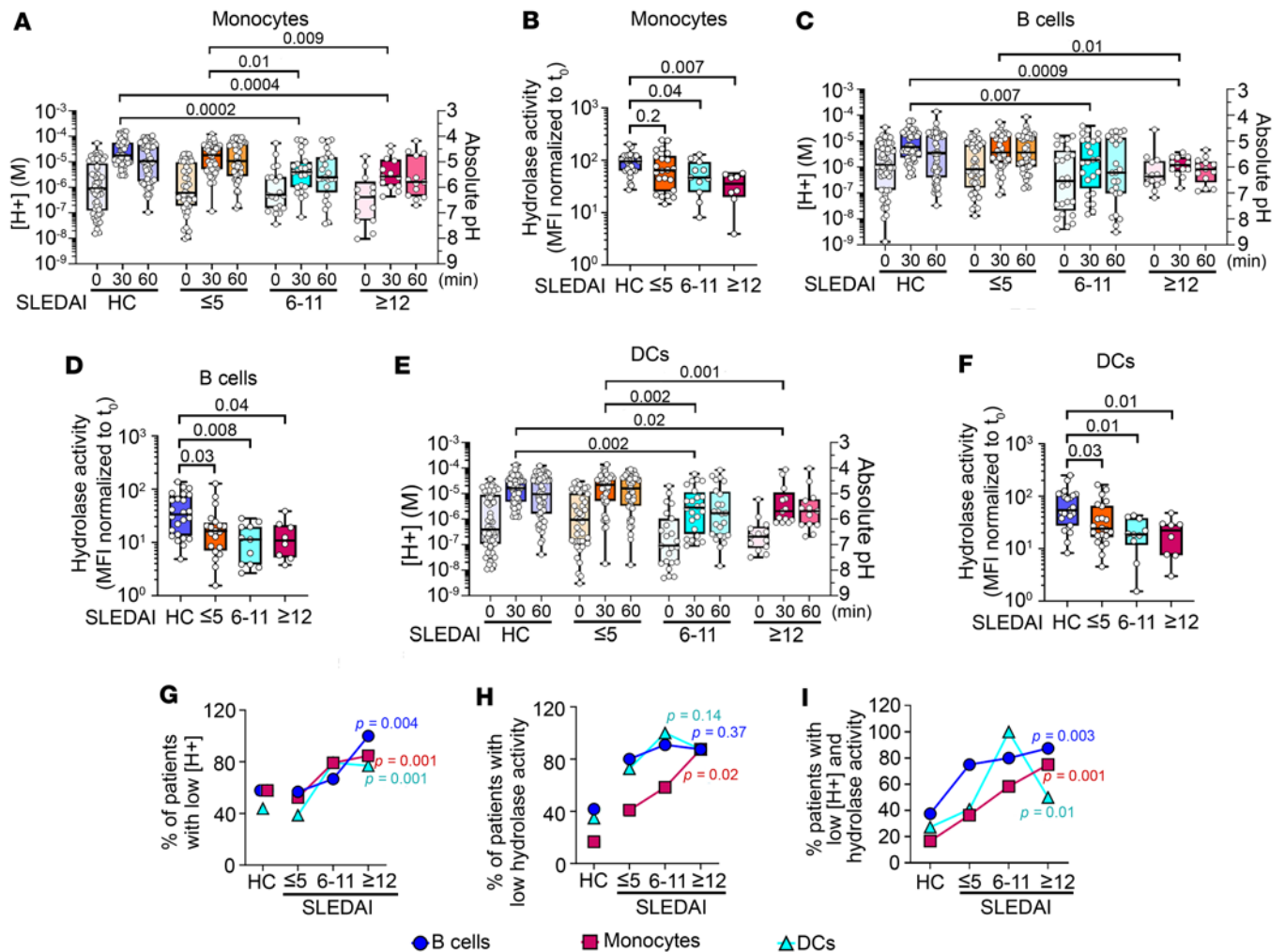


Figure 3. Active SLE patients show diminished LEL acidification and reduced LEL hydrolase activity. Unfractionated blood cells from HCs or SLE patients were stimulated with IgG-ICs (30 μ L IgG-ICs per 0.25×10^6 cells). Unstimulated samples (t_0) were treated with concanamycin A (20 ng/mL) to inhibit vAT-Pase activity. (A–F) At designated times, LEL pH was measured in each cell type (A, C, and E). Absolute pH was calculated using a standard curve. The LEL hydrolase activity was measured by flow cytometry using an acidotropic substrate that fluoresces upon degradation (B, D, and F). The hydrolase substrate MFI was normalized to t_0 . (G–I) Trends were assessed using the Cochran–Armitage test to compare the proportion of patients in each disease group with low [H⁺] (G), low hydrolase activity (H), or low [H⁺] and hydrolase activity (I) for B cells (circles), monocytes (squares), and DCs (triangles). In A, C, and E: HC, N = 57; SLE, N = 81. In B, D, and F: HC, N = 24; SLE, N = 41; more than 8 experiments. Statistical analysis used Kruskal–Wallis (A–F). Adjusted P values with significance are shown. Bars, median; boxes, 25th–75th percentiles; whiskers, minimum and maximum values.

innate cytosolic sensors (27) and endosomal TLRs (28). HCQ also reduces reactive oxygen species (ROS) by blocking NOX2 assembly (29), Ca²⁺ release from the ER (30), and CD40L expression (31), events that decrease cellular activation and the secretion of inflammatory cytokines.

Nuclear self-antigens accumulate on blood Mo, DCs, and B cells during highly active disease. To assess whether SLE patients accumulate nuclear antigens on the plasma membrane, we quantified surface nucleosome on blood cells from SLE patients and HCs. In patients with inactive and moderately active disease, the levels of surface nucleosome on Mo (Figure 4A), B cells (Figure 4B), and DCs (Figure 4C) were comparable to those in HCs. However, in highly active disease, surface nucleosome levels were increased on Mo (1.8-fold), B cells (7.1-fold), and DCs (1.7-fold). Accumulation of surface nuclear antigen on hematopoietic cells was not unique to nucleosome, as highly active SLE patients showed 2.9-fold increased surface dsDNA on Mo ($P = 0.03$) and 5.3-fold increase on B cells ($P \leq 0.0001$) (Supplemental Figure 3, A and B, and Supplemental Table 6). It is also possible that accumulation of surface nucleosome reflected increased Fc γ R expression; however, the levels of Fc γ RI, Fc γ RIIA, Fc γ RIII, and Fc γ RIIb on Mo, DCs, and B cells from SLE patients were not different from HC ($P = 0.23$ – 0.97) (Supplemental Figure 4). It is noteworthy that some of the anti-Fc γ Rs

have epitope specificity for the Fc-binding cleft (blocking antibody) and may not have detected Fc γ Rs that were pre-bound to IgG-ICs. The broad histogram peaks reveal cell-to-cell variability in surface nucleosome, most notably on B cells in highly active disease (Figure 4B). To identify the B cell subset(s) with elevated levels of surface nucleosome, we quantified surface nucleosome on IgD⁺CD27⁻ resting naive (rNAV) B cells, activated naive (aNAV) B cells, and IgD⁻CD27⁻ double-negative 1 (DN1) and 2 (DN2) B cells (Supplemental Figure 5) (32). aNAV B cells are the precursors of DN2 cells that differentiate into antibody-secreting cells through extrafollicular response. The frequencies of rNAV, aNAV, DN1, and DN2 B cells in SLE patient and HC blood showed a significant expansion of aNAV and DN2 cells as previously described (32). Comparing surface nucleosome levels with those in HCs, we found that levels on rNAV B cells were increased 2.0- and 4.4-fold in moderately and highly active disease (Figure 4D), while surface nucleosome on aNAV B cells was increased 4.0-, 4.8-, and 14.6-fold across the SLEDAI groups (Figure 4E). In highly active disease, surface nucleosome on DN2 cells was increased 4.1-fold in comparison with HCs (Figure 4F). Although surface nucleosome was elevated on DN1 cells in highly active disease, the levels were not statistically different from those in HCs ($P = 0.06$; Figure 4G). Thus, during highly active disease, surface nucleosome levels were increased on all cell types; however, the aNAV B cell subset showed the highest levels.

In addition to elevating surface nucleosome, exocytosis also elevates circulating immune complex (CIC) levels. We found that the CIC levels in inactive patients did not change compared with those in HCs; however, in patients with moderately and highly active disease, they were increased 2.2- and 4.7-fold compared with those in HCs ($P = 0.009, 0.0009$) (Figure 4H and Supplemental Table 8). Patients with “high CIC” showed plasma levels higher than a cutoff established at 1.5-fold above the mean CIC level of HCs. The proportion of patients with elevated CIC also increased over the SLEDAI groups, revealing an association between CIC levels and disease activity ($P = 0.01$; Figure 4I). To identify whether increasing disease activity was related to LEL dysfunction, we used Cochran-Armitage analysis. For this analysis, patients with “high surface nucleosome” were defined as having cell levels above a cutoff established at 1.8-fold above the mean surface nucleosome level of HC. We found that a significantly higher proportion of patients in highly active disease showed high surface nucleosome on Mo and B cells (Mo, $P = 0.02$; B cells, $P = 0.003$) (Figure 4J); however, this trend was not seen with DCs ($P = 0.46$). In B cells, the trend was corroborated by a high Spearman’s correlation coefficient in patients with highly active disease ($r = 0.81, P = 0.004$; Supplemental Table 7). We also found that a higher proportion of patients with active disease showed both low [H⁺] and elevated surface nucleosome on B cells ($P = 0.003$), Mo ($P = 0.01$), and DCs ($P = 0.03$; Figure 4K); or high CIC and increased surface nucleosome on B cells ($P = 0.02$) and Mo ($P = 0.001$), but not DCs ($P = 0.52$) (Figure 4L); or elevated CIC and low [H⁺] on B cells ($P = 0.0001$), Mo ($P = 0.001$), and DCs ($P = 0.0001$) (Figure 4M). The weaker trend in DCs could reflect that exocytosis occurs after DCs migrate to lymph nodes and complete their maturation (33), since CICs induce CCR7-dependent migration of DCs to lymph nodes in both human and murine lupus (34). In summary, SLEDAI groups with higher disease activity are associated with decreased hydrolase activity and non-acidic LELs in Mo and B cells, and increased surface nucleosome and CIC on Mo, B cells, and DCs. These findings support the idea that LEL dysfunction associates with SLEDAI groups of higher disease activity.

LEL dysfunction is not evident in active rheumatoid arthritis patients. To assess whether reduced LEL [H⁺] and the accumulation of surface nucleosome were evident in other rheumatic diseases, we analyzed blood hematopoietic cells from active, seropositive rheumatoid arthritis (RA) patients ($n = 23$; Supplemental Table 9). The [H⁺] and levels of surface nucleosome on blood hematopoietic cells from active RA patients were not different in comparison with HCs (Supplemental Figure 6). This indicates that the hallmarks of LEL dysfunction are not evident in blood cells from active RA.

Patients with LEL dysfunction are more likely to have renal disease, rash, and arthritis. To identify relationships between clinical symptoms and LEL dysfunction, we separated patients with non-acidic LELs, then calculated the proportion of this group receiving disease-modifying anti-rheumatic drugs (DMARDs; mycophenolic acid, mycophenolate mofetil, azathioprine, methotrexate, tacrolimus) or having clinical manifestations involving kidneys, skin, or joints. Of the patients with non-acidic LELs, 44% showed current renal disease, 35% SLEDAI rash, and 22% SLEDAI arthritis, and 72% were receiving DMARDs (Supplemental Table 5). In addition, we identified patients with each clinical manifestation (renal, skin, joint, or receiving DMARDs), then calculated the proportion of this subgroup with non-acidic LELs. Of those with current renal disease, rash, or arthritis or receiving DMARDs, 92%, 73%, 63%, and 75%, respectively, had non-acidic LELs (Supplemental Table 4). Thus, when patients show clinical manifestations, they are more

Table 1. Proportion of patients prescribed hydroxychloroquine among patients with acidic versus non-acidic LELs, or with varying disease activity for each cell type

| | Overall | Patients with acidic LEL | Patients with non-acidic LEL ^A | SLEDAI ≤ 5 | SLEDAI 6–11 | SLEDAI ≥ 12 |
|---------------------------------------|---------|--------------------------|-------------------------------------------|------------|-------------|-------------|
| <i>N</i> | 81 | | | | | |
| Patients prescribed HCQ, <i>N</i> (%) | 65 (80) | | | | | |
| Monocytes | | | | | | |
| <i>N</i> | | 28 | 53 | 44 | 24 | 13 |
| Patients prescribed HCQ, <i>N</i> (%) | | 23 (82) | 42 (79) | 36 (82) | 19 (79) | 9 (69) |
| B cells | | | | | | |
| <i>N</i> | | 27 | 54 | 44 | 24 | 13 |
| Patients prescribed HCQ, <i>N</i> (%) | | 20 (74) | 45 (83) | 36 (82) | 19 (79) | 10 (77) |
| DCs | | | | | | |
| <i>N</i> | | 35 | 46 | 44 | 24 | 13 |
| Patients prescribed HCQ, <i>N</i> (%) | | 29 (83) | 36 (78) | 36 (82) | 19 (79) | 10 (77) |

^APatients with non-acidic LELs had [H⁺] lower than the cutoff. For each cell type, the [H⁺] cutoff was established at 1.8-fold above the mean [H⁺] of the HC (monocytes, pH 4.7; B cells, pH 5.1; DCs, pH 4.8). HCQ, hydroxychloroquine.

likely to already exhibit dysfunctional LELs, while patients with non-acidic LELs may not have developed clinical symptoms. This raises the possibility that diminished LEL acidification is coincident with or could precede clinical manifestations.

To identify whether LEL dysfunction associates with renal disease, we grouped SLE patients (regardless of disease activity) into those with active nephritis, those with remission nephritis, and those who never had renal disease (never nephritis), then compared the proportion with non-acidic LELs or increased surface nucleosome. A higher proportion of SLE patients with active renal disease had low [H⁺] (80%–92%; mean SLEDAI of 11) compared with the proportion of patients who never had nephritis (49%–57%) or who had remission nephritis (45%–55%). This suggests that the function of LELs is restored in remission nephritis. Similarly, more patients with active nephritis showed elevated nucleosome on the surface of B cells (48%; Supplemental Table 10). These findings suggest that LEL dysfunction associates with active nephritis and is characterized by low [H⁺] in all cell types and the accumulation of surface nucleosome on Mo, DCs, and B cells from highly active patients. Collectively, our findings show that LEL dysfunction associates with active clinical symptoms (SLEDAI rash, arthritis, and nephritis) and is coincidental with, or could precede, these manifestations.

FcγRI is coupled to LEL dysfunction in MRL/lpr mice. Consistent with a role for FcγRI in murine SLE, we previously showed that MRL/lpr mice lacking FcγRI (FcγRI^{-/-}/MRL/lpr) did not develop lupus and exhibited diminished signaling of phosphorylated Syk^{Y525} (p-Syk^{Y525}), p-Akt^{S473}, p-Akt^{T308}, and p-S6 (13, 14). To assess whether FcγRI^{-/-}/MRL/lpr mice restore LEL function, we used BMMφs and measured acidification ([H⁺]) and ROS. After 30 minutes of stimulation with IgG-ICs, the [H⁺] in MRL/lpr BMMφs was reduced 8.3-fold (*P* = 0.003), while in FcγRI^{-/-}/MRL/lpr BMMφs [H⁺] was only reduced 1.8-fold (*P* = 0.0845) (Figure 5A). The levels of ROS in B6 BMMφs were increased 3.8-fold (*P* < 0.0001) at 15 minutes, returning to 1.4-fold (*P* = 0.288) at 2 hours (Figure 5B). In MRL/lpr BMMφs, ROS were increased 5.8-fold (*P* < 0.0001) at 15 minutes and sustained at 7.3-fold (*P* < 0.0001) at 2 hours (compared with MRL/lpr t₀). In FcγRI^{-/-}/MRL/lpr BMMφs ROS were increased 2.7-fold (*P* = 0.35) at 15 minutes and sustained at 2.7-fold (*P* = 0.707) at 2 hours (compared with FcγRI^{-/-}/MRL/lpr t₀). Thus, loss of FcγRI in MRL/lpr mice reduces the peak ROS levels, but those levels are sustained over 2 hours. We previously identified that FcγRI plays an important role in murine SLE (13), and now show that FcγRI is required for diminished acidification and heightened ROS in MRL/lpr mice, showing a contribution to LEL dysfunction.

Chronic PI3K activity impairs LEL function. Past studies of LEL dysfunction identified a pathway where the binding of cofilin to phagosomal actin is impaired as a result of heightened cofilin phosphorylation. This diminishes Rab39a cleavage (14), a necessary step in lysosomal acidification (35). Since FcγRI is coupled to the cofilin/actin pathway through PI3K/Akt signaling, we tested whether inhibiting PI3K-p110 activity restored LEL function. BMMφs from B6 and MRL/lpr mice were treated with isoform inhibitors of the PI3K-p110 subunit p110α (PIK-75), p110β (TGX-221), or p110δ (IC87114). In MRL/lpr BMMφs,

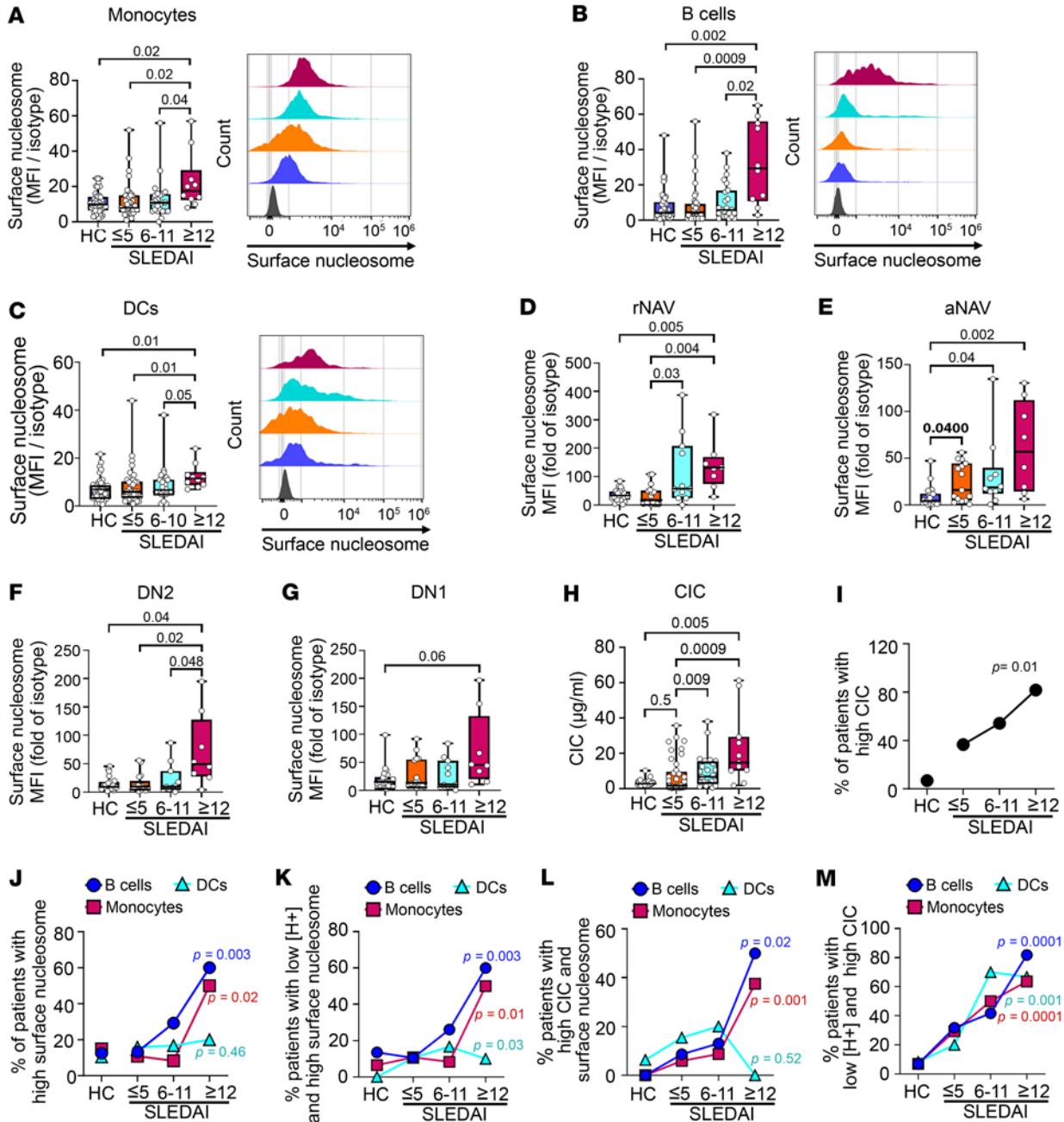


Figure 4. Highly active SLE patients (SLEDAI ≥ 12) show elevated levels of surface nucleosome and circulating immune complexes. (A–G) Unfractionated blood Mo (A), B cells (B), DCs (C), and rNAV (D), aNAV (E), DN2 (F), and DN1 (G) cells were analyzed for surface nucleosome by flow cytometry. Representative histograms show the cell distribution with varying disease activities (gray: isotype control). (H) Plasma circulating immune complex (CIC) levels were measured by IC-mediated internalization of Fc γ RIIA on neutrophils using flow cytometry and a standard curve. $N = 11$ –41 per disease group; 3 experiments. (I–M) Trends were assessed on B cells (circles), Mo (squares), and DCs (triangles) using the Cochran-Armitage test to compare the proportion of patients in each disease group with high CIC (I), high surface nucleosome (J), low $[\text{H}^+]$ and high surface nucleosome (K), high CIC and surface nucleosome (L), and low $[\text{H}^+]$ and high CIC (M). In A–C: HC, $N = 48$; SLE patient, $N = 72$; in D–G: HC, $N = 19$; SLE patient, $N = 8$ –15; 8–48 experiments. Statistical analysis used Kruskal-Wallis (A–H). Adjusted P values with significance are shown. Bars, median; boxes, 25th–75th percentiles; whiskers, minimum and maximum values.

the $[\text{H}^+]$ was decreased 9.2-fold ($P < 0.0001$) in comparison with B6 t_{30} (Figure 5C). In MRL/*lpr* BMM ϕ s, the p110 α inhibitor did not restore an acidic $[\text{H}^+]$, instead maintaining 3.9-fold decreased $[\text{H}^+]$ ($P = 0.0001$) in comparison with B6 t_{30} . In contrast, treatment with inhibitors of p110 β or p110 δ increased the $[\text{H}^+]$ to levels comparable to B6 t_{30} levels (1.1-fold, $P = 0.2503$; 1.1-fold, $P = 0.2812$). Inhibiting PI3K-p110 β or -p110 δ , but not PI3K-p110 α , in MRL/*lpr* BMM ϕ s also prevented exocytosis (Figure 5D). The levels of fluoro-chrome-tagged IgG-ICs on MRL/*lpr* BMM ϕ s were 3.8-fold higher than those on untreated B6 BMM ϕ s

($P = 0.0389$). However, after treatment with p110 β or p110 δ inhibitors, [H⁺] levels were comparable or below the levels in B6 BMM ϕ s. In contrast, the levels of exocytosis in MRL/*lpr* BMM ϕ s treated with the p110 α inhibitor were not different from those in untreated MRL/*lpr* ($P = 0.5$). These data demonstrate that chronic PI3K activity of p110 β and p110 δ in MRL/*lpr* BMM ϕ s contributes to diminished LEL acidification and reduced degradation of IgG-ICs. It also corroborates previous data showing reduced lupus nephritis, B cell expansion, BAFF, and autoantibody production in Fc γ RI^{-/-}/MRL/*lpr* mice (13).

To understand how PI3K activity contributes to LEL dysfunction, we analyzed the products of PI3K activation in IgG-IC-stimulated B6 and MRL/*lpr* BMM ϕ s. PI3K activation converts PI(4,5)P₂ to PI(3,4,5)P₃ (PIP₃) (Figure 5E). In B6 BMM ϕ s, basal levels of PIP₃ increased 2.5-fold ($P = 0.013$) after 15 minutes of stimulation, then returned to basal levels. In MRL/*lpr* BMM ϕ s, basal levels of PIP₃ were increased 1.6-fold (compared with B6 t_0). Following 15 minutes of stimulation, PIP₃ levels further increased 1.4-fold ($P = 0.179$) to levels that were 2.3-fold ($P = 0.04$) higher than B6 t_0 . At 6 hours, PIP₃ levels remained relatively high at 1.7-fold ($P = 0.08$) compared with B6 t_0 . The elevated basal levels, and low IgG-IC-induced levels, of PIP₃ suggest sustained PI3K activity in MRL/*lpr* mice. Alternatively, diminished phosphatase activity could heighten PIP₃. To gain insight into phosphatases regulating PIP₃ levels, we examined other phosphoinositide products. Activation of SHIP-1 dephosphorylates PIP₃ to produce PI(3,4)P₂ (36). PI(3,4)P₂ levels were transiently increased over 1 hour (1.8-fold, $P \leq 0.0001$) in B6 BMM ϕ s, but unchanged in MRL/*lpr* (1.0-fold, $P = 0.79$) (Figure 5F). Reduced formation of PI(3,4)P₂ following IgG-IC stimulation of MRL/*lpr* BMM ϕ s suggests impaired SHIP-1 activity.

To assess whether phosphorylation of SHIP-1 reflected the phosphoinositide products, we compared levels of p-SHIP-1^{Y1022} in B6 and MRL/*lpr* BMM ϕ s (Figure 5G). B6 BMM ϕ s increased p-SHIP-1^{Y1022} 1.9-fold ($P \leq 0.0001$ compared with B6 t_0) after 1 hour of stimulation, which returned to baseline by 5 hours. Unstimulated MRL/*lpr* BMM ϕ s had slightly higher basal p-SHIP-1^{Y1022} (1.25-fold, $P = 0.74$ compared with B6) that remained unchanged over 5 hours (1.2-fold; $P > 0.99$ compared with MRL/*lpr* t_0). The results support the idea that impaired SHIP-1 phosphorylation could account for the sustained PIP₃ levels in MRL/*lpr* BMM ϕ s. They also raised the possibility that impaired phosphorylation of SHIP-1 in MRL/*lpr* BMM ϕ s could reflect decreased recruitment of SHIP-1 to the plasma membrane to localize with Fc γ RIIb (36). To assess this, we used confocal microscopy to quantify the levels of p-SHIP-1^{Y1022} colocalized with cholera toxin-stained (CTx-stained) membrane lipid rafts (Figure 5, H–J). Following 1 hour of stimulation with IgG-ICs, the levels of p-SHIP-1^{Y1022} colocalized with CTx-positive lipid rafts on the plasma membrane of MRL/*lpr* BMM ϕ s (Figure 5I) were 2.7-fold decreased ($P < 0.0001$) compared with B6 (Figure 5J). Taken together, these results demonstrate that MRL/*lpr* BMM ϕ s show decreased SHIP-1 phosphorylation and fail to localize p-SHIP-1 to the lipid rafts and the site of Fc γ RI.

Diminished SHIP activity in non-autoimmune mice partially impairs LEL function. Src homology 2-containing inositol phosphatase-1 (SHIP-1; *Inpp5d*) is activated by phosphorylation at Y¹⁰²² (37) and recruited to Fc γ RI through ITIM-containing Fc γ RIIb. We hypothesized that if SHIP-1 was unable to efficiently dephosphorylate PIP₃ in MRL/*lpr* BMM ϕ s and consequently induce LEL dysfunction, then B6 BMM ϕ s deficient in SHIP-1 (B6.SHIP-1^{-/-}) should recapitulate LEL dysfunction in MRL/*lpr* mice. Following stimulation with IgG-ICs, B6.SHIP-1^{-/-} BMM ϕ s showed a 3.7-fold decrease ($P = 0.01$) in [H⁺] at 30 minutes, while MRL/*lpr* showed a 10.3-fold decrease ($P < 0.0001$) (compared with B6 t_0), suggesting that SHIP-1 deficiency does not fully recapitulate diminished acidification in MRL/*lpr* mice (Figure 6A). Similarly, at 60 minutes after stimulation, the B6.SHIP-1^{-/-} BMM ϕ s did not show increased [H⁺], confirming that delayed acidification was not occurring (data not shown). When BMM ϕ s were stimulated with IgG-ICs for 15 minutes, ROS levels in B6.SHIP-1^{-/-} BMM ϕ s increased 3.3-fold ($P = 0.03$) in comparison with B6.SHIP-1^{-/-} at t_0 , while MRL/*lpr* showed 2.1-fold increase ($P = 0.03$) and B6 showed 2.0-fold increase ($P = 0.03$) in comparison with their individual t_0 (Figure 6B). At 2 hours, ROS declined in B6.SHIP-1^{-/-} (1.6-fold, $P = 0.72$) and B6 (1.3-fold, $P = 0.28$) BMM ϕ s compared with their individual t_0 , while in MRL/*lpr*, ROS levels remained high (2.0-fold, $P = 0.04$). This indicates that SHIP-1 deficiency does not recapitulate the elevated levels of sustained ROS seen in MRL/*lpr* mice. We then assessed whether SHIP-1 deficiency increased exocytosis of undegraded IgG-ICs (Figure 6C). MRL/*lpr* BMM ϕ s showed slightly higher levels (1.2-fold) of fluorochrome-labeled IgG-ICs at 72 hours compared with preloaded levels at t_0 ($P = 0.76$), indicating exocytosis of IgG-ICs to the plasma membrane (Figure 6C and Figure 2C). In contrast, B6 and B6.SHIP-1^{-/-} BMM ϕ s showed surface fluorescence comparable to or below t_0 , consistent with IgG-IC degradation. Like B6.SHIP-1^{-/-}, B6 BMM ϕ s treated with a SHIP-1 inhibitor (3AC) showed modestly decreased [H⁺] and significantly elevated but not sustained ROS, with no exocytosis (Figure 6, A–C). Together, the data show that the SHIP-1 deficiency is not sufficient to recapitulate the LEL dysfunction of MRL/*lpr* mice.

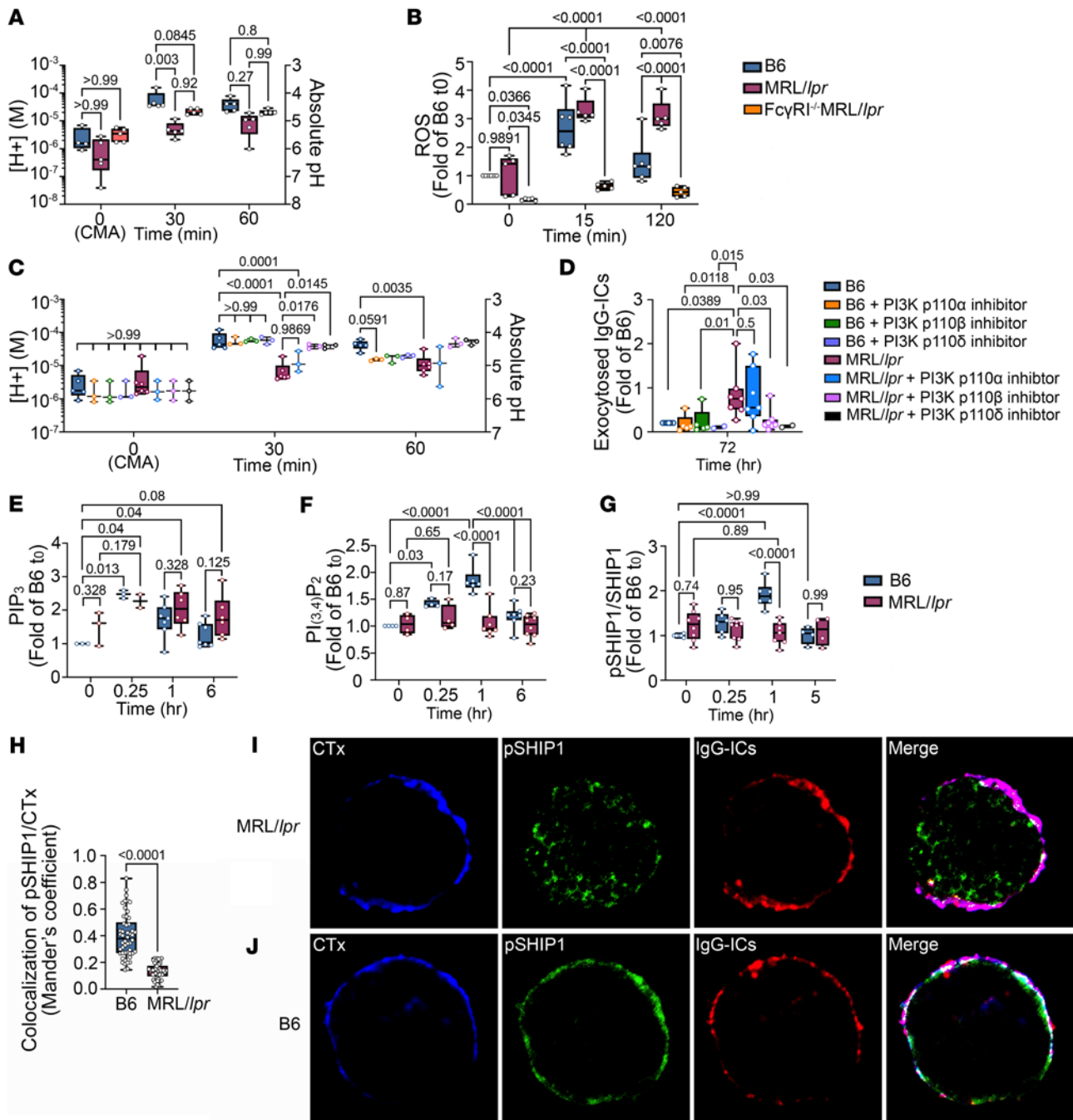


Figure 5. LEL defects are induced by chronic PI3K activation and SHIP-1 defects and evident in *FcγRI^{-/-}/MRL/lpr* mice. (A–J) BMMφs were stimulated with IgG-ICs (25 μL IgG-ICs per 0.25 × 10⁶ cells). At designated times, LEL pH (A and C), ROS (B), exocytosis (D), PIP₃ (E), PI(3,4)P₂ (F), and p-SHIP-1^{Y1022} (G) were measured by flow cytometry. vATPase activity in unstimulated samples [*t*₀(CMA)] was inhibited with concanamycin A (CMA; 2 ng/mL) (A and C). ROS levels (B) were measured using CellROX including *t*₀ samples untreated with IgG-ICs. BMMφs were preloaded (*t*₀) with Alexa Fluor 488-labeled IgG-ICs, and exocytosis was measured at designated times (C). Surface-bound fluorescence was assessed by subtraction of internalized fluorescence (surface quenched) from total (unquenched) and normalized to individual *t*₀. The effect of PI3K was measured using PI3K-p110 inhibitors (p110α, β, and δ) (100 nM, 2 hours before IgG-IC treatment) (C and D). The colocalization of IgG-ICs (red) and p-SHIP-1^{Y1022} (green) with cholera toxin-positive lipid rafts (CTx, blue) (H) in BMMφs was analyzed by confocal microscopy (I and J). Images were processed using ImageJ (NIH). Representative images are shown. White in merged images depicts colocalized IgG-ICs, p-SHIP-1^{Y1022}, and CTx. Statistical analysis used 2-way ANOVA with multiple comparisons (A–G) and Mann-Whitney test (H). Adjusted *P* values with significance are shown. *N* = 2–8, 2–5 experiments (A–H); *N* = 3, 3 experiments, total of 50 cells per mouse line (H–J). Bars, median; boxes, 25th–75th percentiles; whiskers, minimum and maximum values.

SHIP-1 (*Ptprb*), a protein tyrosine phosphatase that dephosphorylates the FcγR γ chain (FcRγ; FCER1G) immunoreceptor tyrosine-based activation motif (ITAM) (YxxL/I) (38), decreases Syk recruitment (39) and dampens FcγRI signal transduction (40). If heightened PI3K activity in LEL dysfunction occurs

through sustained Fc γ RI signaling, then B6.SHP-1-deficient mice (B6.SHP-1^{fl/fl} \times B6.Rosa26-CreERT2) should recapitulate the LEL defect seen in MRL/*lpr* BMM ϕ s. Tamoxifen treatment of SHP-1-deficient mice efficiently excised SHP-1 (Supplemental Figure 7). Following 30 minutes of stimulation with IgG-ICs, B6.SHP-1^{-/-} BMM ϕ s showed 3.9-fold ($P = 0.03$) lower [H⁺] compared with 10.3-fold ($P = 0.0003$) lower in MRL/*lpr* (compared with B6 t_{30} ; Figure 6D). After 15 minutes of IgG-IC stimulation, acute ROS levels in B6.SHP-1^{-/-} BMM ϕ s were increased 6.5-fold ($P = 0.02$) compared with a 2.1-fold ($P = 0.03$) increase in MRL/*lpr* (Figure 6E). At 2 hours, sustained ROS in B6.SHP-1^{-/-} BMM ϕ s were 8.5-fold over t_0 ($P = 0.005$), while levels in MRL/*lpr* were sustained at 2.0-fold ($P = 0.04$), indicating that SHP-1 deficiency heightens and sustains ROS. B6.SHP-1^{-/-} BMM ϕ s did not show exocytosis of undegraded IgG-ICs (Figure 6F). Like the B6.SHP-1^{-/-} BMM ϕ s, B6 BMM ϕ s treated with an SHP-1 inhibitor (NSC-87877) showed modestly decreased [H⁺], slightly elevated acute ROS, and no exocytosis (Figure 6, D–F). Together, the data show that SHP-1 deficiency or inhibitors of SHP-1 activity are not sufficient to fully recapitulate the LEL dysfunction of MRL/*lpr* mice.

Phosphorylation of SHP-1 at Y⁵⁶⁴ (p-SHP-1) is necessary for phosphatase activity (41). Stimulation of B6 and MRL/*lpr* BMM ϕ s with IgG-IC (15 minutes to 5 hours) induced comparable p-SHP-1^{Y564} at all time points (Supplemental Figure 8A). Since Fc γ RI constitutively resides within lipid rafts (42), SHP-1 must localize to lipid rafts to dephosphorylate the Fc γ RI ITAM (43). We used confocal microscopy to assess colocalization of p-SHP-1^{Y564} with CTx-stained membrane lipid rafts in B6 and MRL/*lpr* BMM ϕ s following IgG-IC stimulation. We found comparable colocalization of p-SHP-1^{Y564} with lipid rafts in B6 and MRL/*lpr* BMM ϕ s (Supplemental Figure 8, B and C). Thus, reduced SHP-1 phosphorylation, or intracellular pSHP-1^{Y564} mislocalization, does not impair LEL function in MRL/*lpr* BMM ϕ s.

Reduced SHIP-1 and SHP-1 activity impairs LEL function. To assess whether deficiency in both SHP-1 and SHIP-1 recapitulates LEL dysfunction in MRL/*lpr* mice, we treated B6.SHP-1^{-/-} BMM ϕ s with the SHP-1/2 inhibitor NSC-87877. After stimulation with IgG-ICs (30 minutes), B6.SHP-1^{-/-} BMM ϕ s treated with SHP-1/2 inhibitor showed 4.5-fold ($P = 0.05$) lower [H⁺], while MRL/*lpr* BMM ϕ s showed 10.3-fold ($P = 0.0001$) lower [H⁺], compared with B6 t_{30} (Figure 6G). Further, B6.SHP-1^{-/-} BMM ϕ s treated with SHP-1/2 inhibitor showed a 2.7-fold increase in ROS (15 minutes, $P = 0.04$), while MRL/*lpr* BMM ϕ s showed a 2.1-fold ($P = 0.03$) increase compared with untreated cells (Figure 6H). Sustained ROS (2 hours) in B6.SHP-1^{-/-} BMM ϕ s treated with SHP-1/2 inhibitor were also elevated (2.2-fold increase, $P = 0.065$), while MRL/*lpr* levels were increased 2.0-fold ($P = 0.04$). Although treatment of B6.SHP-1^{-/-} BMM ϕ s with SHP-1/2 inhibitor diminished acidification and heightened ROS, it did not induce exocytosis of undegraded IgG-ICs (Figure 6I).

To corroborate these findings, we treated B6.SHP-1^{-/-} BMM ϕ s with SHIP-1 inhibitor (3AC). Compared with B6, IgG-IC stimulation of B6.SHP-1^{-/-} BMM ϕ s with SHIP-1 inhibitor showed a 9.1-fold lower [H⁺] at 30 minutes ($P = 0.003$), while [H⁺] was 10.3-fold increased in MRL/*lpr* BMM ϕ s ($P = 0.0001$; Figure 6G). Additionally, B6.SHP-1^{-/-} BMM ϕ s treated with SHIP-1 inhibitor for 15 minutes showed 8.4-fold heightened ROS ($P = 0.002$), while MRL/*lpr* showed 2.1-fold ($P = 0.03$; Figure 6H). Levels of sustained ROS (2 hours) were 10.7-fold increased in B6.SHP-1^{-/-} BMM ϕ s treated with SHIP-1 inhibitor ($P = 0.001$), whereas they were 2.0-fold increased in MRL/*lpr* ($P = 0.04$). The dual deficiency of SHP-1 and SHIP-1 induced a 2.6-fold increase in the exocytosis of undegraded IgG-ICs ($P = 0.02$; Figure 6I). Thus, LEL dysfunction in B6.SHP-1^{-/-} BMM ϕ s treated with SHIP-1 inhibitor recapitulated MRL/*lpr*, while B6.SHP-1^{-/-} with SHP-1/2 inhibitor was less effective. One possibility is that although heightened ROS is necessary, it is not sufficient to drive LEL dysfunction, while diminished acidification plays a more important role. Collectively, the data show that defects in SHP-1 and SHIP-1 contribute to LEL dysfunction in MRL/*lpr* mice, suggesting that these phosphatases play direct or indirect roles in disabling LEL function in lupus. Whether other phosphatases in the PI3K/Akt pathway, such as PTEN or Akt phosphatases (PP2A, PHLPP1/2), also play similar roles is unclear.

Discussion

Our murine studies show that activation of PI3K, in part through chronic Fc γ R signaling, results from, and leads to, diminished LEL acidification, creating a feedforward loop (13–15). In human disease, non-acidic LELs and increased circulating and membrane-bound IgG-ICs are evident during active disease, while acidic LELs and low levels of circulating and membrane-bound IgG-ICs prevail during inactive disease. This is consistent with the idea that LEL dysfunction could drive active versus inactive disease. In further

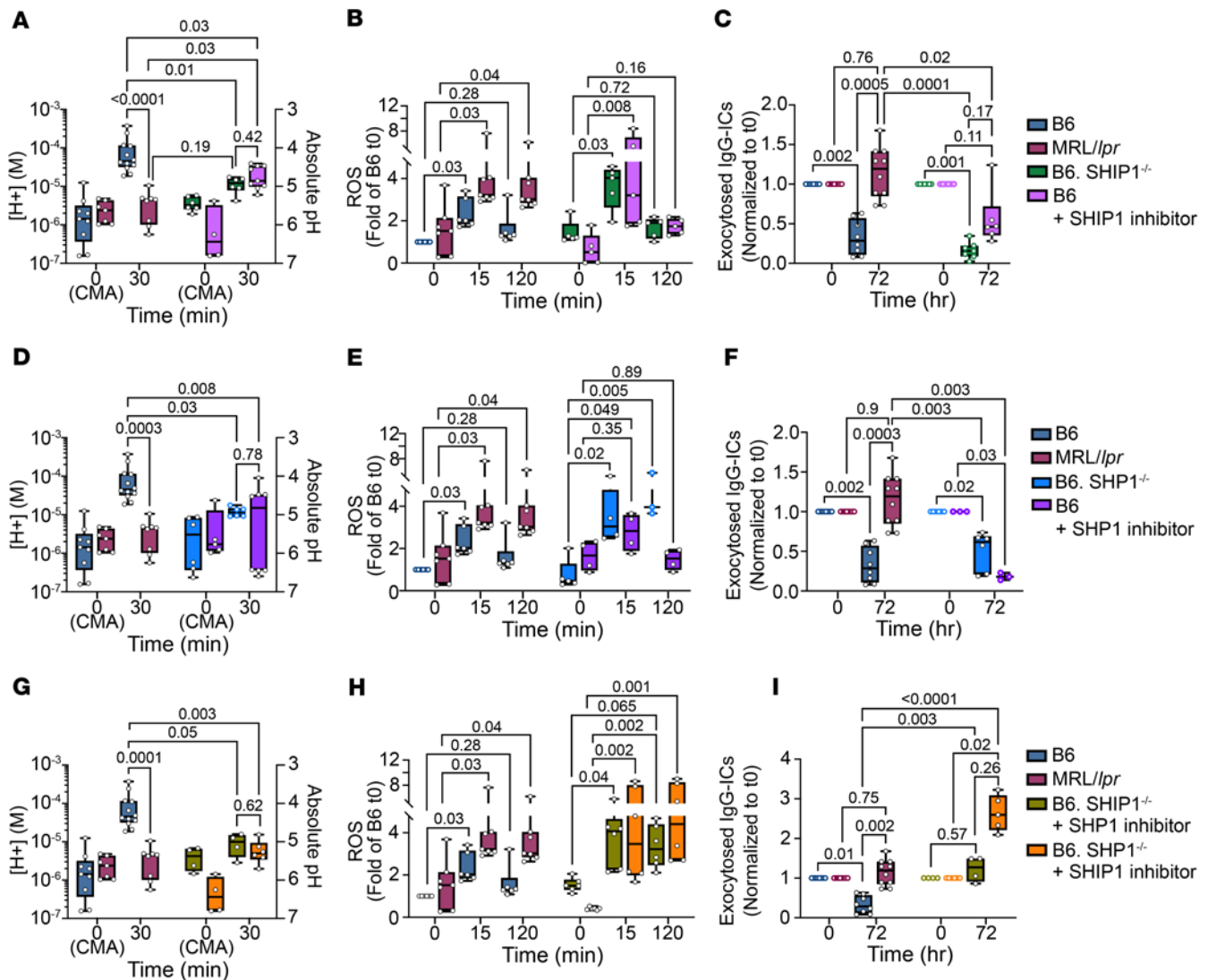


Figure 6. Deficiency in SHP-1 and inhibition of SHIP-1 in B6 mice phenocopy the LEL dysfunction seen in MRL/lpr. To assess the effects of SHIP-1 and/or SHP-1 on LEL defects, BMMφs from B6, B6.SHIP-1^{-/-}, and B6.SHP-1^{-/-} mice were treated or not treated with inhibitors of SHP-1 (10 μM NSC-87877, 3 hours before IgG-IC treatment) or SHIP-1 (50 nM 3AC, 48 hours before IgG-IC treatment). The effects of single deficiency of SHIP-1 (A–C) or SHP-1 (D–F) or double deficiency (G and H) were analyzed. BMMφs were stimulated with IgG-ICs (25 μL IgG-ICs per 0.25 × 10⁶ cells) with or without inhibitors. At designated times, LEL pH (A, D, and G), ROS (B, E, and H), and exocytosis (C, F, and I) were measured by flow cytometry. Absolute pH was calculated using a standard curve (A, D, and G). vATPase activity in unstimulated samples [*t*₀(CMA)] was inhibited with concanamycin A (CMA; 2 ng/mL). ROS levels (B, E, and H) were measured using CellROX including *t*₀ samples untreated with IgG-ICs, and fold of B6 *t*₀ was graphed. BMMφs were preloaded (*t*₀) with Alexa Fluor 488-labeled IgG-ICs, and exocytosis was measured at designated times (C, F, and I). Surface-bound fluorescence was assessed by subtraction of internalized fluorescence (surface quenched) from total (unquenched) and normalized to individual *t*₀. Statistical analysis used Kruskal-Wallis test with multiple comparisons. Adjusted *P* values with significance are shown. *N* = 4–12; 3–4 experiments. Bars, median; boxes, 25th–75th percentiles; whiskers, minimum and maximum values.

support of that idea, we find that diminished [H⁺] and hydrolase activity are evident in patients with moderate and highly active SLE (Figure 3), yet the accumulation of surface nucleosome and increased CICs are predominantly seen in highly active disease (Figure 4). These data suggest that non-acidic LELs decrease the degradation of IgG-ICs, which in turn promotes exocytosis and heightens CICs and the accumulation of undegraded IgG-ICs on the plasma membrane (9). Thus, LEL dysfunction is unlikely the “cause” of lupus, but rather is likely an induced defect that perpetuates disease (Figure 5, C and D). This is supported by genome-wide association studies and twin studies demonstrating genetic underpinnings in SLE (1, 44). Clinically, LEL dysfunction is associated with increasing SLE disease activity (Figure 3, G–I, and Figure 4, I–M) and is coincident with, or may precede, clinical manifestations of SLEDAI rash, arthritis, and nephritis (Supplemental Table 4). Non-acidic LELs are evident in 67% of SLE patients (65% Mo, 57% DCs), raising the possibility that restoring LEL function could be a therapeutic target that sustains inactive disease.

Murine studies showed that diminished LEL acidification is induced through PI3K activation (Figure 5, C and D). This suggests that heritability of LEL dysfunction could originate from genes conferring indirect effects that disrupt cellular signaling networks required to regulate immune responses (45). The data also suggest that Fc γ RI signaling, induced by newly formed IgG-ICs, or those that have accumulated on the cell surface, is not properly terminated and chronically activates the PI3K/Akt/mTORC pathway (Figure 5). Chronic activation of Fc γ RI/PI3K/Akt/mTOR that heightens ROS and reduces acidification is also sustained by disrupted regulation by SHP-1 and SHIP-1, phosphatases that normally attenuate Fc γ RI signal transduction (Figure 6). Genetic polymorphisms could also disrupt LEL function. Transient ROS production by nicotinamide adenine dinucleotide phosphate (NADPH) oxidase is important for LEL maturation and acidification (46), deficiency in NOX2 exacerbates murine SLE (47), and genetic risk variants of NCF that lower ROS promote lupus in non-autoimmune mice (48, 49). In contrast, heightened and/or prolonged ROS impairs the activity of lysosomal hydrolases (50), diminishes activity of protein tyrosine phosphatases through oxidation at the catalytic site of protein (51), and diminishes phagosomal acidification by disrupting vATPase assembly (52). Thus, ROS are tightly regulated to allow transient increases that are appropriately terminated. In summary, genetic and induced events can disrupt LEL function in SLE, with our human and murine data revealing a potential mechanism underlying an induced defect.

In non-autoimmune B6 mice, deficiency in both SHIP-1 and SHP-1 is sufficient to reduce LEL acidification, heighten ROS, and promote exocytosis of undegraded IgG-ICs (Figure 6, G–I). SHP-1 dephosphorylates Y⁵⁸ within the ITAM of Fc γ R and multiple signaling effectors that regulate Fc γ R signaling, including the Src family kinases p-Syk, p-62Dok, and p-Vav. One possible mechanism by which SHP-1 might contribute to LEL dysfunction in MRL/*lpr* mice is through reduced phosphatase activity due to high ROS that chronically oxidize the SHP-1 catalytic site, thereby limiting dephosphorylation of Fc γ RI ITAM tyrosines and/or other receptor-proximal signaling effectors.

SHIP-1 also plays a crucial role in LEL dysfunction in MRL/*lpr* mice (Figure 5, E–J, and Figure 6, A–C). SHIP-1 regulates the levels of PIP₃, which acts as a docking site for kinases (53) regulating Fc γ RI activation at the level of PI3K activation (Figure 5E). In MRL/*lpr* mice, diminished phosphorylation of SHIP-1 could prevent Fc γ RIIb/SHIP-1 colocalization with Fc γ RI-containing lipid rafts. This would sustain PIP₃ levels and induce LEL dysfunction. Exclusion of Fc γ RIIb/SHIP-1 from lipid rafts might occur through mutations within the Fc γ RIIb transmembrane region (54, 55), or through altered composition of glycosphingolipids, as in CD4⁺ T cell lipid rafts from SLE patients (56). Last, we did not see a decrease in SHIP-1 total protein; thus, we do not think microRNA regulation of SHIP-1 is involved.

How does LEL dysfunction occur in lymphocytes that do not typically express activating Fc γ Rs? LEL dysfunction in B cells could involve Fc γ RIIb and surface receptors that bind apoptotic debris, like autoreactive B cell receptors, or receptors that bind opsonins such as complement, oxidized LDL, Gas6, or milk fat globule epidermal growth factor 8. In B cells, late endosomes are the preferred site for degrading endocytic cargo (57), and accumulation of undegraded nucleic acid drives TLR7 pathologies in SLE (58, 59). T cells also do not typically express activating Fc γ R; however, autophagy defects (60) affect T cell metabolism and mitochondrial function (61, 62). Autophagy requires functional LELs to degrade intracellular waste. A therapeutic phospho-peptide derived from the spliceosomal U1-70K protein reduces chaperone-mediated autophagy and limits T cell activation and plasma cell formation in murine and human SLE (63). In summary, LEL defects are evident in both murine and human lupus and inducible via chronic Fc γ RI/PI3K/Akt/mTOR signaling from newly formed and/or exocytosed IgG-ICs. The sustained activation of the PI3K pathway is (or could be) in part due to disrupted SHIP-1 and SHP-1 function. Thus, a feedforward loop, created when elevated IgG-ICs chronically activate Fc γ R/PI3K signaling, reduces LEL acidification, heightens ROS, and sustains IgG-IC levels through exocytosis of undegraded LEL cargo, setting in motion a sustained cycle of LEL dysfunction and inflammation.

Study limitations include the relatively low enrollment of Hispanic and Asian patients and the cross-sectional nature of the study. We chose hybrid SELENA-SLEDAI as the disease activity marker because it is a validated, reliable, objective SLE disease activity measure that is easy to score and not confounded by fibromyalgia. The well-accepted disadvantages of SLEDAI are insensitivity to small change and inability to capture severity within each category. The strengths of this study are that our demographics reflect the overall SLE population with a predominance of Black women; we enrolled SLE and RA patients from 2 sites; and SLE patients were grouped based on disease activity (inactive, moderately active, highly active).

Methods

Sex as a biological variable

For human studies, sex was not considered as a biological variable. For studies with animals, both sexes were used since both male and female MRL/*lpr* mice develop spontaneous lupus.

Study design and demographics

Peripheral blood hematopoietic cells were analyzed at the University of North Carolina (UNC). At the time of visit, disease activity was scored using hybrid SELENA-SLEDAI (64). Disease activity and demographic data were entered into UNC or Duke University REDCap databases and are provided in Supplemental Tables 2, 6, and 9. SELENA-SLEDAI or 28-joint Disease Activity Score (DAS28) scores were not available until after laboratory data were analyzed, and the clinical investigators were blinded to the results of the study until final data analysis was completed. No duplicate patients were used in the study.

Patient enrollment criteria

Consenting patients who met the 1997 American College of Rheumatology (ACR) or 2012 SLICC criteria for SLE (65) were enrolled. Exclusion criteria (prospective) included age under 18 years, chronic infection, active malignancy, inability to provide informed consent, or having received rituximab within 6 months and intravenous Ig, belimumab, or a biologic medication for rheumatic disease (including anti-TNF therapy) within 3 months. The inclusion criteria for rheumatoid arthritis (RA) were that patients (a) met ACR RA criteria, (b) showed seropositivity for RF or CCP, (c) showed activity as measured by DAS28 ESR ≥ 3.2 or DAS28 CRP ≥ 2.9 , (d) had at least 1 joint with synovitis, and (e) were not on biologics or small-molecule therapy. Healthy controls (HCs) were enrolled through the UNC Platelet Donation Center or Duke OB-GYN clinic and selected as those without family history of autoimmune disorders or current symptoms of infection.

Animal models

We obtained C57BL/6 (B6), MRL/MpJ-*Tnfrsf6^{lpr}*/J (MRL/*lpr*; 000485), MRL/MpJ (000486), and B6.MRL-Fas^{lpr}/J (B6.*lpr*; 000482) mice from The Jackson Laboratory; C57BL/6-*Gt(ROSA)26Sor^{tm9(Cre/ESR1)Ar}* (B6.Rosa26-CreERT2; 10471) from Taconic Biosciences; and B6.SHP-1^{fl/fl} mice from Paul Love (NIH, Bethesda, Maryland, USA). Fc γ RI^{-/-}/MRL/*lpr* mice were previously described (13). When mice reached a disease endpoint described in the IACUC protocol, they were euthanized following IACUC guidelines.

Reagents and antibodies

A list of reagents and antibodies is provided in Supplemental Methods.

IgG-immune complexes

IgG-immune complexes (IgG-ICs) were made from apoptotic blebs obtained by irradiation of B6 thymocytes (7- to 9-week-old mice) or CCRF-CEM human thymoma cells (180×10^6 ; ATCC CCL-119) at 6 Gy in 10 mL of PBS plus 2% FBS. After incubation (16–18 hours), supernatants containing apoptotic debris were collected from centrifuged (350g) cultures. Depending on sample number, a given volume of the apoptotic debris was incubated with 12 μ g/mL of PL2-3 (IgG2a) (13) for 1 hour (mouse study) or 12 μ g/mL 33H11 (IgG1) (66) for 2 hours (human study) at room temperature. IgG-ICs were pelleted by centrifuging at 160,000g for 45 minutes at 4°C, and resuspended in complete medium (10% FBS, 1 mM sodium pyruvate, 50 μ g/mL gentamicin, 100 U/mL penicillin, 100 μ g/mL streptomycin, 2 mM L-glutamine, and 5×10^{-5} M β -mercaptoethanol in phenol red-free RPMI for human samples or phenol red-free DMEM for mouse samples) at 25% of the volume that was used in binding PL2-3/33H11. To stimulate cells, we used 25 or 30 μ L of IgG-ICs per 0.25×10^6 cells.

Flow cytometry

RBC-lysed blood cells from human samples and mouse splenocytes and BMM ϕ s were stained for surface-bound and intracellular targets using standard methods for flow cytometry (Supplemental Methods).

To inhibit PI3K-p110 subunit isoforms, BMM ϕ s were treated with 100 nM of PIK-75 (which inhibits p110 α with 13-fold higher specificity than p110 γ), TGX-221 (which inhibits p110 β with 20-fold higher

specificity than p110 δ), and IC87114 (which inhibits p110 δ with 58-fold higher specificity than p110 γ), 2 hours before IgG-IC treatment. To inhibit SHIP-1, we used 3AC (50 nM) on day 5 (48 hours before IgG-IC treatment), and for SHP-1, we used NSC-87877 (10 μ M) at 3 hours before IgG-ICs treatment. To generate SHP-1-deficient BMM ϕ s, B6.SHP-1^{fl/fl} \times B6.Rosa26-CreERT2 mice were treated with tamoxifen (2 mg in 100 μ L corn oil, i.p.) for 4 consecutive days, and then at 17 days after first injection of tamoxifen, bone marrow cells were collected and cultured as described above. SHIP-1-deficient BMM ϕ s were generated from the bones of B6.SHIP-1^{-/-} mice provided by Gerald Krystal (British Columbia Cancer Agency, Vancouver, British Columbia, Canada). We obtained spleens and bones of NZM2410 mice from Melissa Cunningham (Medical University of South Carolina, Charleston, South Carolina, USA), and of B6.Sle123 mice from Laurence Morel (University of Texas, San Antonio, Texas, USA).

Late endosome/lysosome pH. Unfractionated RBC-lysed human blood cells or mouse splenocytes/BMM ϕ s (0.25×10^6) were stained for cell markers (Supplemental Methods). Cells were stimulated with IgG-ICs (25 or 30 mL of IgG-ICs per 0.25×10^6 cells) for 30 minutes at 37°C, and then LEL pH was measured. Samples were washed and resuspended in 200 μ L of warmed complete medium for 60 minutes, then continued incubating at 37°C for 30 minutes. To establish time 0 (t_0), the vATPase was inhibited using concanamycin A (human, 20 ng/mL; mouse, 2 ng/mL). To measure pH changes, LysoSensor 160-DND (1 μ L/sample) was added 15 minutes before flow cytometry. LysoSensor was excited with a UV laser (355 nm), and relative pH was calculated by ratioing of the MFI from 2 emission channels (450/20 nm, 585/42 nm). Linear regression from the standard curve of each cell type was used to calculate absolute pH, followed by conversion to hydrogen ion concentration ($[H^+]$) based on $pH = -\log_{10}[H^+]$. The standard curve was generated using intracellular pH calibration buffer.

Late endosome/lysosome hydrolase activity. Late endosomal/lysosomal hydrolase activity was measured using a hydrolase activity kit with a modified protocol. In brief, cells were treated with IgG-ICs (30 μ L of IgG-ICs per 0.25×10^6 cells) and the self-quenched substrate provided in the kit (Lysosomal Intracellular Activity Assay kit, ab234622, Abcam) (15 μ L/1 mL) for 60 minutes at 37°C. After washing, cells were left at room temperature for 45 minutes, then analyzed by flow cytometry. The MFI at 488 nm reflected hydrolase activity. Relative hydrolase activity was calculated by subtraction of MFI of fluorescence minus one (FMO) for FITC, then normalized to concanamycin A-treated sample (t_0).

ROS. Intracellular ROS levels were measured using a CellROX Deep Red kit (C10491, Thermo Fisher Scientific) with modified protocol. In brief, while BMM ϕ s were treated with IgG-ICs (25 μ L of IgG-ICs per 0.25×10^6 cells) for 15 and 120 minutes, CellROX (1 μ M) was added with antibodies against cell markers 15 minutes before the end of IgG-IC treatment. Cells were stained with a Live/Dead kit (L34994, Thermo Fisher Scientific), then fixed in 2% paraformaldehyde/FACS buffer. Samples without IgG-IC stimulation were t_0 samples. ROS levels were calculated by subtraction of MFI of FMO from MFI of CellROX-stained samples.

Exocytosis of fluorochrome-labeled IgG-ICs to plasma membrane. IgG-ICs were made with apoptotic debris and Alexa Fluor 488-labeled (AF488-labeled) PL2-3. BMM ϕ s were preloaded with AF488-labeled IgG-ICs for 30 minutes at 4°C, and unbound IgG-ICs were removed by washing. After incubation at 37°C for 24 and 72 hours (with or without inhibitors for some experiments), half of the samples were treated with anti-AF488 antibody to quench surface-bound AF488 fluorescence, and the other half were left unquenched. To set t_0 , cells preloaded with AF488-labeled IgG-ICs were processed the same way with anti-AF488 without further incubation. All samples were then fixed and analyzed by flow cytometry. MFI from quenched samples indicates fluorescence from internalized IgG-ICs, and MFI of unquenched samples depicts total fluorescence from both surface-bound and internalized IgG-ICs. Levels of exocytosed IgG-ICs were calculated by subtraction (internalized and surface fluorescence minus internalized fluorescence). MFI of exocytosed IgG-ICs was normalized to individual t_0 .

Circulating immune complexes. The concentration of circulating immune complexes (CICs) was quantified by measurement of the loss of Fc γ RIIA when HC neutrophils were incubated with patient (or HC) plasma (67). Plasma was separated on the day of blood collection, aliquoted, and stored at -80°C until analysis. Neutrophils were isolated from HC blood using Polymorphprep (NC0863559, Fisher Scientific). After RBC lysis with ACK buffer, 0.2×10^6 cells per 180 μ L of phenol red-free RPMI were plated into 96-well U-bottom plates, and 20 μ L of patient plasma was added to each well (final 10%). Plates were incubated (37°C, 90 minutes) to allow for internalization of the plasma immune complexes. To stop internalization, cells were washed with cold FACS buffer containing 0.2% of NaN₃, then stained with fixable

Live/Dead. To measure surface expression of Fc γ RIIA, cells were stained with fluorochrome-conjugated IV.3 (anti-Fc γ RIIA) and antibodies against cell markers, then fixed. We measured the MFI of IV.3 staining on CD45⁺CD14⁻HLA-DR⁻CD16⁺CD11b⁺CD15⁺ neutrophils. The concentration of plasma CICs was calculated using a standard curve generated by treatment of cells with various concentrations of heat-aggregated IgG-ICs (human 33H11 heated 1 hour at 63°C).

Samples were acquired on a Thermo Fisher Scientific Attune NxT flow cytometer or a Cytex Aurora system (5 lasers). Lysosome pH and hydrolase activity data were obtained for the human study on a Becton Dickinson LSRFortessa and for the murine study on a Becton Dickinson LSRII. Data acquired from Cytex Aurora were unmixed using SpectroFlo. All flow cytometry data were analyzed with FlowJo and graphed using GraphPad Prism.

Confocal microscopy

We used confocal microscopy to measure colocalization of cholera toxin-stained membrane lipid rafts with intracellular p-SHIP-1^{Y1022} or p-SHP-1^{Y564} (Supplemental Methods). Quantitative data of colocalization were obtained by calculation of Mander's coefficient of colocalization (colocalized pixels/total fluorescent pixels within region of interest).

Statistics

Murine data were analyzed using the non-parametric 2-way ANOVA, Kruskal-Wallis, or Mann-Whitney test with original false discovery rate (FDR) method (Benjamini-Hochberg [BH]) for multiple comparisons (GraphPad Prism v9.5.1). For human data, we used the Shapiro-Wilk test, visual inspection of Q-Q plots, and Levene's test to assess homogeneity of variance to assess normality of data. We used Dunn (1964) Kruskal-Wallis non-parametric ANOVA adjusted for FDR (BH), followed by pairwise comparisons to assess the differences between 4 disease groups (HCs, and SLE patients with hybrid SELENA-SLEDAI [SLEDAI] of ≤ 5 , 6–11, or ≥ 12). Cochran-Armitage test was used to identify trends between the proportion of patients in each disease activity group and parameters associated with LEL dysfunction ([H⁺], hydrolase, surface nucleosome, CIC). The *P* values were adjusted for multiple comparisons (BH method). Fold change is used in the text for ease of comparison between SLEDAI groups; however, fold change was not used in calculating *P* values. The statistical methods for calculating *P* values are provided in each figure legend and were done between all groups or experimental conditions, but only 2-sided *P* values less than 0.05 were considered statistically significant. Associations between SLEDAI groups and the presence of diminished [H⁺] and hydrolase activity, or elevated surface nucleosome and circulating immune complexes, were defined by cutoffs: Patients with “non-acidic” lysosomes had [H⁺] lower than the cutoff. The cutoff for each cell type was established at 1.8-fold above the mean [H⁺] of the HC. Patients with “low-hydrolase” had levels below a cutoff that was established at 1.7-fold above the mean hydrolase of HCs for each cell type. Patients with “high surface nucleosome” had cell surface nucleosome levels above the cutoff. The cutoffs for each cell type were established at 1.8-fold above the mean surface nucleosome level of the HC. Patients with “high CIC” showed plasma CIC levels higher than the cutoff. The cutoff was established at 1.5-fold above the mean CIC level of the HC. These defined thresholds are also described in the legend to Supplemental Table 4. Clinical categories were described with mean \pm SD for continuous variables, and *N* (%) for binary categorical variables. The study was not powered for comparisons between clinical categories, so these comparisons were not made, to avoid inflating type II error.

Study approval

Primary Institutional Review Board (IRB) oversight was the responsibility of the UNC Office of Human Research Ethics with approval of the consent form and protocols for the study by the Duke University Health System IRB for Clinical Investigations. Participants were enrolled under approved UNC IRBs (12-2097, 18-3193, 19-1690) and Duke IRBs (Pro00008875, Pro0000775, Pro00094645, Pro00080944). During routine clinic visits, patients who provided written consent were enrolled. This study was approved by the UNC Institutional Animal Care and Use Committee (IACUC; 21-136, 24-092).

Data availability

All experimental data are shown in the main text or the supplemental materials and are provided in the Supporting Data Values file.

Author contributions

SK, JLR, and BJV designed the study. SK and AJM conducted experiments and acquired and analyzed data. JLR (Duke) and SZS (UNC) identified patients. KG (Duke), SSB, and ACT (UNC) obtained consent from patients. KG, SSB, ACT, and XB procured samples. KS, RES, MM, MEBC, JLR (Duke), and SZS (UNC) supported patient enrollment, SLEDAI scoring, clinical data interpretation, and overall guidance on human SLE disease. BJV and JLR oversaw the project. LA performed statistical analysis. SK and BJV wrote the manuscript. We determined the order of authorship based on the levels of contribution to the project.

Funding support

This work is supported by NIH funding, in whole or part, and is subject to the NIH Public Access Policy. Through accepting this federal funding, the NIH has been given a right to make the work publicly available in PubMed Central.

- National Institutes of Health (NIH) 1R01AI132421-01A1 (BJV, JLR, MEBC).
- NIH P30CA016086, 1UM2AI30836-01, 5P30AI05041 (Flow Cytometry Core).
- NIH Center for Clinical Research P30AR072580 (Thurston Arthritis Center–Statistical Core).
- NIH National Center for Advancing Translational Sciences Clinical and Translational Science Award UL1TR002489 (REDCap data management).
- Lupus Research Alliance Novel Research Grant (BJV, JLR).
- Department of Defense Lupus Research Program (BJV, SZS).
- North Carolina Biotechnology Center, Biotechnology Innovation Grant (BJV).
- North Carolina Biotechnology Center IDG-1025 (Flow Cytometry Core).
- Rosemarie K. Witter Foundation Inc., gift (BJV).

Acknowledgments

We thank Amanda Nelson for critically reviewing the manuscript; the Duke and UNC Lupus Registries and the SLE patients who provided blood for this study; the UNC Platelet Donation Center and staff for providing healthy control blood; the UNC Microscopy Services Laboratory; Thomas H. Winkler (FAU, Erlangen, Germany) for providing 33H11 (anti-DNA) hybridoma; QuanZhen Li (University of Texas Southwestern, Dallas, Texas, USA) for confirming specificity of 33H11; Christian Lood (University of Washington, Seattle, Washington, USA) for advice establishing the flow-based CIC assay; and Edna Scarlett and Julie Walker for managing the Duke and UNC IRBs. The Graphical Abstract was created with BioRender.com.

Address correspondence to: Barbara J. Vilen, Department of Microbiology and Immunology, University of North Carolina at Chapel Hill, Chapel Hill, North Carolina 27599, USA. Email: barb_vilen@med.unc.edu.

AJM's present address is: Department of Microbiology, University of Tennessee, Knoxville, Tennessee, USA.

-
1. Chen L, et al. Genetic advances in systemic lupus erythematosus: an update. *Curr Opin Rheumatol*. 2017;29(5):423–433.
 2. Tsokos GC, et al. New insights into the immunopathogenesis of systemic lupus erythematosus. *Nat Rev Rheumatol*. 2016;12(12):716–730.
 3. Owen KA, et al. Deconvoluting the heterogeneity of SLE: the contribution of ancestry. *J Allergy Clin Immunol*. 2022;149(1):12–23.
 4. Lovgren T, et al. Induction of interferon-alpha production in plasmacytoid dendritic cells by immune complexes containing nucleic acid released by necrotic or late apoptotic cells and lupus IgG. *Arthritis Rheum*. 2004;50(6):1861–1872.
 5. Hargraves MM, et al. Presentation of two bone marrow elements; the tart cell and the L.E. cell. *Proc Staff Meet Mayo Clin*. 1948;23(2):25–28.
 6. Mahajan A, et al. Clearance deficiency and cell death pathways: a model for the pathogenesis of SLE. *Front Immunol*. 2016;7:35.
 7. Ahuja A, et al. An acquired defect in IgG-dependent phagocytosis explains the impairment in antibody-mediated cellular depletion in lupus. *J Immunol*. 2011;187(7):3888–3894.
 8. Colonna L, et al. Beyond apoptosis in lupus. *Curr Opin Rheumatol*. 2014;26(5):459–466.
 9. Buratta S, et al. Lysosomal exocytosis, exosome release and secretory autophagy: the autophagic- and endo-lysosomal systems go extracellular. *Int J Mol Sci*. 2020;21(7):2576.
 10. Diering GH, Numata M. Endosomal pH in neuronal signaling and synaptic transmission: role of Na⁽⁺⁾/H⁽⁺⁾ exchanger NHE5. *Front Physiol*. 2014;4:412.
 11. Pillay CS, et al. Endolysosomal proteolysis and its regulation. *Biochem J*. 2002;363(pt 3):417–429.
 12. Johnson DE, et al. The position of lysosomes within the cell determines their luminal pH. *J Cell Biol*. 2016;212(6):677–692.

13. Kang S, et al. Apoptotic debris accumulates on hematopoietic cells and promotes disease in murine and human systemic lupus erythematosus. *J Immunol.* 2016;196(10):4030–4039.
14. Monteith AJ, et al. mTORC2 activity disrupts lysosome acidification in systemic lupus erythematosus by impairing caspase-1 cleavage of Rab39a. *J Immunol.* 2018;201(2):371–382.
15. Monteith AJ, et al. Defects in lysosomal maturation facilitate the activation of innate sensors in systemic lupus erythematosus. *Proc Natl Acad Sci U S A.* 2016;113(15):E2142–E2151.
16. Bergtold A, et al. FcR-bearing myeloid cells are responsible for triggering murine lupus nephritis. *J Immunol.* 2006;177(10):7287–7295.
17. Lee JH, et al. Faulty autolysosome acidification in Alzheimer's disease mouse models induces autophagic build-up of A β in neurons, yielding senile plaques. *Nat Neurosci.* 2022;25(6):688–701.
18. Zeng J, et al. Restoration of lysosomal acidification rescues autophagy and metabolic dysfunction in non-alcoholic fatty liver disease. *Nat Commun.* 2023;14(1):2573.
19. Platt FM, et al. Lysosomal storage diseases. *Nat Rev Dis Primers.* 2018;4(1):27.
20. Adler LN, et al. The other function: class II-restricted antigen presentation by B cells. *Front Immunol.* 2017;8:319.
21. Rudofsky UH, et al. Differences in expression of lupus nephritis in New Zealand mixed H-2z homozygous inbred strains of mice derived from New Zealand black and New Zealand white mice. Origins and initial characterization. *Lab Invest.* 1993;68(4):419–426.
22. Morel L, et al. Genetic reconstitution of systemic lupus erythematosus immunopathology with polycongenic murine strains. *Proc Natl Acad Sci U S A.* 2000;97(12):6670–6675.
23. Petri M, et al. Classification and definition of major flares in SLE clinical trials. *Lupus.* 1999;8(8):685–691.
24. Humbert M, et al. Major histocompatibility complex class II-restricted presentation of secreted and endoplasmic reticulum resident antigens requires the invariant chains and is sensitive to lysosomotropic agents. *Eur J Immunol.* 1993;23(12):3167–3172.
25. Lu S, et al. Lysosomal adaptation: how cells respond to lysosomotropic compounds. *PLoS One.* 2017;12(3):e0173771.
26. Parker FS, Irvin JL. The interaction of chloroquine with nucleic acids and nucleoproteins. *J Biol Chem.* 1952;199(2):897–909.
27. An J, et al. Cutting edge: Antimalarial drugs inhibit IFN- β production through blockade of cyclic GMP-AMP synthase-DNA interaction. *J Immunol.* 2015;194(9):4089–4093.
28. Kuznik A, et al. Mechanism of endosomal TLR inhibition by antimalarial drugs and imidazoquinolines. *J Immunol.* 2011;186(8):4794–4804.
29. Muller-Calleja N, et al. Hydroxychloroquine inhibits proinflammatory signalling pathways by targeting endosomal NADPH oxidase. *Ann Rheum Dis.* 2017;76(5):891–897.
30. Goldman FD, et al. Hydroxychloroquine inhibits calcium signals in T cells: a new mechanism to explain its immunomodulatory properties. *Blood.* 2000;95(11):3460–3466.
31. Wu SF, et al. Hydroxychloroquine inhibits CD154 expression in CD4⁺ T lymphocytes of systemic lupus erythematosus through NFAT, but not STAT5, signaling. *Arthritis Res Ther.* 2017;19(1):183.
32. Jenks SA, et al. Distinct effector B cells induced by unregulated Toll-like receptor 7 contribute to pathogenic responses in systemic lupus erythematosus. *Immunity.* 2018;49(4):725–739.
33. Kim MK, Kim J. Properties of immature and mature dendritic cells: phenotype, morphology, phagocytosis, and migration. *RSC Adv.* 2019;9(20):11230–11238.
34. Clatworthy MR, et al. Immune complexes stimulate CCR7-dependent dendritic cell migration to lymph nodes. *Nat Med.* 2014;20(12):1458–1463.
35. Seto S, et al. Rab GTPases regulating phagosome maturation are differentially recruited to mycobacterial phagosomes. *Traffic.* 2011;12(4):407–420.
36. Ono M, et al. Role of the inositol phosphatase SHIP in negative regulation of the immune system by the receptor Fc(gamma)RIIB. *Nature.* 1996;383(6597):263–266.
37. Lamkin TD, et al. Shc interaction with Src homology 2 domain containing inositol phosphatase (SHIP) in vivo requires the Shc-phosphotyrosine binding domain and two specific phosphotyrosines on SHIP. *J Biol Chem.* 1997;272(16):10396–10401.
38. Meng TC, et al. Reversible oxidation and inactivation of protein tyrosine phosphatases in vivo. *Mol Cell.* 2002;9(2):387–399.
39. Yamashita T, et al. Differential dephosphorylation of the FcRgamma immunoreceptor tyrosine-based activation motif tyrosines with dissimilar potential for activating Syk. *J Biol Chem.* 2008;283(42):28584–28594.
40. Mkaddem SB, et al. Lyn and Fyn function as molecular switches that control immunoreceptors to direct homeostasis or inflammation. *Nat Commun.* 2017;8(1):246.
41. Frank C, et al. Effective dephosphorylation of Src substrates by SHP-1. *J Biol Chem.* 2004;279(12):11375–11383.
42. Beekman JM, et al. FcgammaRI (CD64) resides constitutively in lipid rafts. *Immunol Lett.* 2008;116(2):149–155.
43. D'Ambrosio D, et al. Recruitment and activation of PTP1C in negative regulation of antigen receptor signaling by Fc gamma RIIB1. *Science.* 1995;268(5208):293–297.
44. Block SR, et al. Studies of twins with systemic lupus erythematosus. A review of the literature and presentation of 12 additional sets. *Am J Med.* 1975;59(4):533–552.
45. Boyle EA, et al. An expanded view of complex traits: from polygenic to omnigenic. *Cell.* 2017;169(7):1177–1186.
46. Bagaitkar J, et al. NADPH oxidase activation regulates apoptotic neutrophil clearance by murine macrophages. *Blood.* 2018;131(21):2367–2378.
47. Campbell AM, et al. NADPH oxidase inhibits the pathogenesis of systemic lupus erythematosus. *Sci Transl Med.* 2012;4(157):157ra141.
48. Geng L, et al. Human SLE variant *NCF1*-R90H promotes kidney damage and murine lupus through enhanced Th2 responses induced by defective efferocytosis of macrophages. *Ann Rheum Dis.* 2022;81(2):255–267.
49. Meng Y, et al. The *NCF1* variant p.R90H aggravates autoimmunity by facilitating the activation of plasmacytoid dendritic cells. *J Clin Invest.* 2022;132(16):e153619.
50. Rybicka JM, et al. NADPH oxidase activity controls phagosomal proteolysis in macrophages through modulation of the luminal redox environment of phagosomes. *Proc Natl Acad Sci U S A.* 2010;107(23):10496–10501.

51. Abram CL, Lowell CA. Shp1 function in myeloid cells. *J Leukoc Biol.* 2017;102(3):657–675.
52. Song SB, Hwang ES. High levels of ROS impair lysosomal acidity and autophagy flux in glucose-deprived fibroblasts by activating ATM and Erk pathways. *Biomolecules.* 2020;10(5):761.
53. Marshall AJ, et al. Regulation of B-cell activation and differentiation by the phosphatidylinositol 3-kinase and phospholipase Cgamma pathway. *Immunol Rev.* 2000;176:30–46.
54. Kono H, et al. FcgammaRIIB Ile232Thr transmembrane polymorphism associated with human systemic lupus erythematosus decreases affinity to lipid rafts and attenuates inhibitory effects on B cell receptor signaling. *Hum Mol Genet.* 2005;14(19):2881–2892.
55. Floto RA, et al. Loss of function of a lupus-associated FcgammaRIIB polymorphism through exclusion from lipid rafts. *Nat Med.* 2005;11(10):1056–1058.
56. McDonald G, et al. Normalizing glycosphingolipids restores function in CD4⁺ T cells from lupus patients. *J Clin Invest.* 2014;124(2):712–724.
57. Lautwein A, et al. Human B lymphoblastoid cells contain distinct patterns of cathepsin activity in endocytic compartments and regulate MHC class II transport in a cathepsin S-independent manner. *J Leukoc Biol.* 2004;75(5):844–855.
58. Lau CM, et al. RNA-associated autoantigens activate B cells by combined B cell antigen receptor/Toll-like receptor 7 engagement. *J Exp Med.* 2005;202(9):1171–1177.
59. Pisitkun P, et al. Autoreactive B cell responses to RNA-related antigens due to TLR7 gene duplication. *Science.* 2006;312(5780):1669–1672.
60. Caza T, et al. Cell type-specific mechanistic target of rapamycin-dependent distortion of autophagy pathways in lupus nephritis. *Transl Res.* 2022;245:55–81.
61. Morel L. Immunometabolism in systemic lupus erythematosus. *Nat Rev Rheumatol.* 2017;13(5):280–290.
62. Zhao L, et al. Mitochondrial impairment and repair in the pathogenesis of systemic lupus erythematosus. *Front Immunol.* 2022;13:929520.
63. Bonam SR, et al. Autophagy: a new concept in autoimmunity regulation and a novel therapeutic option. *J Autoimmun.* 2018;94:16–32.
64. Petri M, et al. Combined oral contraceptives in women with systemic lupus erythematosus. *N Engl J Med.* 2005;353(24):2550–2558.
65. Tan EM, et al. The 1982 revised criteria for the classification of systemic lupus erythematosus. *Arthritis Rheum.* 1982;25(11):1271–1277.
66. Winkler TH, et al. IgG human monoclonal anti-DNA autoantibodies from patients with systemic lupus erythematosus. *Clin Exp Immunol.* 1991;85(3):379–385.
67. Bengtsson AA, et al. Neutrophil FcγRIIA availability is associated with disease activity in systemic lupus erythematosus. *Arthritis Res Ther.* 2020;22(1):126.